Received: 18 January 2018 | Revised: 15 April 2018 | Accepted: 18 April 2018

DOI: 10.1111/gcb.14297

PRIMARY RESEARCH ARTICLE

WILEY Global Change Biology

Solar-induced chlorophyll fluorescence is strongly correlated with terrestrial photosynthesis for a wide variety of biomes: First global analysis based on OCO-2 and flux tower observations

Xing Li[1,2] | Jingfeng Xiao[1] | Binbin He[2,3] | M. Altaf Arain[4] | Jason Beringer[5] | Ankur R. Desai[6] | Carmen Emmel[7] | David Y. Hollinger[8] | Alisa Krasnova[9] | Ivan Mammarella[10] | Steffen M. Noe[9] | Penélope Serrano Ortiz[11] | A. Camilo Rey-Sanchez[12] | Adrian V. Rocha[13] | Andrej Varlagin[14]

[1]Earth Systems Research Center, Institute for the Study of Earth, Oceans, and Space, University of New Hampshire, Durham, New Hampshire

[2]School of Resources and Environment, University of Electronic Science and Technology of China, Chengdu, China

[3]Center for Information Geoscience, University of Electronic Science and Technology of China, Chengdu, China

[4]McMaster Centre for Climate Change and School of Geography and Earth Sciences, McMaster University, Hamilton, ON, Canada

[5]The UWA school of Agriculture and Environment, The University of Western Australia, Crawley, WA, Australia

[6]Department of Atmospheric and Oceanic Sciences, University of Wisconsin-Madison, Madison, Wisconsin

[7]Department of Environmental Systems Science, Institute of Agricultural Sciences, ETH Zurich, Zurich, Switzerland

[8]Northern Research Station, USDA Forest Service, Durham, New Hampshire

[9]Institute of Agricultural and Environmental Sciences, Estonian University of Life Sciences, Tartu, Estonia

[10]Faculty of Science, Institute for Atmosphere and Earth System Research/Physics, University of Helsinki, Helsinki, Finland

[11]Instituto Interuniversitario de Investigación del Sistema Tierra en Andalucía (IISTA-CEAMA), Universidad de Granada, Granada, Spain

[12]Department of Civil, Environmental and Geodetic Engineering, The Ohio State University, Columbus, Ohio

[13]Department of Biological Sciences and the Environmental Change Initiative, University of Notre Dame, Notre Dame, Indiana

[14]A.N. Severtsov Institute of Ecology and Evolution, Russian Academy of Sciences, Moscow, Russia

Correspondence
Jingfeng Xiao, Earth Systems Research Center, Institute for the Study of Earth, Oceans, and Space, University of New Hampshire, Durham, NH 03824.
Email: j.xiao@unh.edu

Funding information
National Aeronautics and Space Administration, Grant/Award Number: NNX14AJ18G, NNX16AG61G; National Science Foundation, Grant/Award Number: 1065777, 1638688; Iola Hubbard Climate Change Endowment; National Natural Science Foundation of China, Grant/Award Number: 41471293, 41671361; China Scholarship Council

Abstract

Solar-induced chlorophyll fluorescence (SIF) has been increasingly used as a proxy for terrestrial gross primary productivity (GPP). Previous work mainly evaluated the relationship between satellite-observed SIF and gridded GPP products both based on coarse spatial resolutions. Finer resolution SIF (1.3 km × 2.25 km) measured from the Orbiting Carbon Observatory-2 (OCO-2) provides the first opportunity to examine the SIF–GPP relationship at the ecosystem scale using flux tower GPP data. However, it remains unclear how strong the relationship is for each biome and whether a robust, universal relationship exists across a variety of biomes. Here we conducted the first global analysis of the relationship between OCO-2 SIF and tower GPP for a total of 64 flux sites across the globe encompassing eight major biomes. OCO-2 SIF showed strong correlations with tower GPP at both midday and daily timescales, with the strongest relationship observed for daily SIF at the 757 nm ($R^2 = 0.72$, $p < 0.0001$). Strong linear relationships between SIF and GPP were consistently

found for all biomes (R^2 = 0.57–0.79, $p < 0.0001$) except evergreen broadleaf forests (R^2 = 0.16, $p < 0.05$) at the daily timescale. A higher slope was found for C_4 grasslands and croplands than for C_3 ecosystems. The generally consistent slope of the relationship among biomes suggests a nearly universal rather than biome-specific SIF–GPP relationship, and this finding is an important distinction and simplification compared to previous results. SIF was mainly driven by absorbed photosynthetically active radiation and was also influenced by environmental stresses (temperature and water stresses) that determine photosynthetic light use efficiency. OCO-2 SIF generally had a better performance for predicting GPP than satellite-derived vegetation indices and a light use efficiency model. The universal SIF–GPP relationship can potentially lead to more accurate GPP estimates regionally or globally. Our findings revealed the remarkable ability of finer resolution SIF observations from OCO-2 and other new or future missions (e.g., TROPOMI, FLEX) for estimating terrestrial photosynthesis across a wide variety of biomes and identified their potential and limitations for ecosystem functioning and carbon cycle studies.

KEYWORDS
carbon cycle, carbon flux, chlorophyll fluorescence, eddy covariance, gross primary productivity, MODIS, OCO-2, vegetation type

1 | INTRODUCTION

Gross primary productivity (GPP), the amount of carbon assimilated by plants through photosynthesis, is the largest carbon flux between the terrestrial biosphere and the atmosphere. Accurate quantification of GPP has important implications for understanding ecosystem functions, carbon cycling, and feedbacks to the climate. The recent advent of satellite-based measurement of solar-induced chlorophyll fluorescence (SIF) has provided tremendous potential for monitoring terrestrial photosynthesis globally (Frankenberg et al., 2011, 2014; Joiner, Yoshida, Vasilkov, & Middleton, 2011; Joiner et al., 2013). Some previous studies have examined the relationship of SIF measured from space with gridded GPP data products at coarse spatial resolutions (Guanter et al., 2012; Parazoo et al., 2014) and more recently with ecosystem-level GPP estimates from eddy covariance (EC) flux towers (Li, Xiao, & He, 2018a; Verma et al., 2017; Wood et al., 2017). However, the relationship between SIF and GPP across a variety of biomes is still unclear mainly due to the scale mismatch between satellite and flux tower footprints and the lack of finer resolution SIF data and concurrent flux tower observations.

SIF is essentially a "glow" of plants under sunlight, and is an energy flux emitted from plant chlorophyll molecules a few nanoseconds after light absorption in the wavelength range from 600 to 800 nm (Baker, 2008). Light energy absorbed by the leaf chlorophyll molecules has three different pathways: photochemistry, nonphotochemical quenching (NPQ, i.e., heat dissipation), and a small fraction re-emitted as SIF (Baker, 2008). SIF is highly correlated with photosynthesis when NPQ dominates at high light levels (Baker, 2008). SIF is directly linked to the actual plant photochemistry and is therefore more physiologically based than the traditional vegetation indices (VIs) such as the normalized difference vegetation index (NDVI) and the enhanced vegetation index (EVI) (Meroni et al., 2009; Zarco-Tejada, Morales, Testi, & Villalobos, 2013). VIs are more indicative of vegetation "greenness" and are less sensitive to actual variations in photosynthesis (Grace et al., 2007; Zhang et al., 2016). SIF can be expressed in a similar way as the light use efficiency (LUE) approach (Monteith, 1972; Monteith & Moss, 1977) for estimating GPP. The LUE approach can be expressed as follows:

$$\mathrm{GPP} = f\mathrm{PAR} \times \mathrm{PAR} \times \mathrm{LUE}_p = \mathrm{APAR} \times \mathrm{LUE}_p \quad (1)$$

where *f*PAR is the fraction of photosynthetically active radiation (PAR) absorbed by vegetation canopies (typically approximated by MODIS VIs or based on satellite-derived *f*PAR data products), APAR is the PAR absorbed by vegetation canopies (*f*PAR × PAR), and $\mathrm{LUE_p}$ denotes photosynthetic light use efficiency. SIF can be similarly expressed (Yoshida et al., 2015) as follows:

$$\mathrm{SIF} = f\mathrm{PAR} \times \mathrm{PAR} \times \mathrm{SIF}_{\mathrm{yield}} = \mathrm{APAR} \times \Theta_f \times \Omega_c \quad (2)$$

where $\mathrm{SIF_{yield}}$ is the emitted SIF per photon absorbed, the product of the fluorescence yield at the membrane scale Θ_f and a structural interference factor Ω_c. $\mathrm{SIF_{yield}}$ determines the fraction of SIF photons escaping the canopy.

The ability of satellite-derived SIF to monitor terrestrial photosynthesis has been investigated since global SIF products became available (Frankenberg et al., 2014; Guanter et al., 2012; Joiner et al., 2011, 2013; Li, Xiao, & He, 2018b; Zhang et al., 2014). Commonly used SIF measurements are derived from the Greenhouse Gases Observing Satellite (GOSAT), the Global Ozone Monitoring Mission

Experiment-2 (GOME-2), and the SCanning Imaging Absorption SpectroMeter for Atmospheric ChartographY (SCIAMACHY). Strong linear correlation has been observed between SIF from GOSAT and GOME-2 and gridded GPP data, suggesting that SIF is a promising proxy for GPP at large scales (Frankenberg et al., 2011; Guanter et al., 2012, 2014; Koffi, Rayner, Norton, Frankenberg, & Scholze, 2015; Li et al., 2018b; Parazoo et al., 2014). Other studies have also shown that SIF has a better performance in detecting plant phenology and water stress than conventional VIs such as NDVI and EVI (Jeong et al., 2017; Joiner et al., 2014; Lee et al., 2013; Sun et al., 2015; Walther et al., 2016; Yoshida et al., 2015). However, these satellite-derived SIF products have coarse spatial resolutions (e.g., GOME-2: 40 × 80 km^2; GOSAT: 10 km diameter; SCIAMACHY: 30 × 240 km^2), and have a large scale mismatch with the footprint of typical EC flux towers (with longitudinal dimensions ranging from a few hundred meters to several kilometers; Schmid, 2002). The scale mismatch hinders the direct linking of satellite-derived SIF and EC tower-based GPP estimates (hereafter tower GPP) at the ecosystem scale (Li et al., 2018a). Currently, this problem can be addressed by the release of finer resolution SIF products from NASA's Orbiting Carbon Observatory-2 (OCO-2) (Frankenberg et al., 2014; Li et al., 2018a).

The OCO-2, launched on July 2, 2014, has enabled retrievals of SIF with much smaller footprints (i.e., 1.3 km × 2.25 km) and slightly higher signal-to-noise ratios with an orbital track (Frankenberg et al., 2014). The midday local overpass time (1:30 p.m.) of OCO-2 is similar to that of GOSAT but with much greater measurement frequency (Frankenberg et al., 2014). The footprint of OCO-2 is close to that of EC flux towers, and therefore the observatory provides the first opportunity to directly link satellite-derived SIF to flux tower GPP at the ecosystem scale. Several pioneering studies have examined the relationship between OCO-2 SIF and tower GPP at individual sites including crops (Wood et al., 2017), grassland (Verma et al., 2017), and temperate forests (Li et al., 2018a), demonstrating strong relationships between OCO-2 SIF and tower GPP for these biomes. Combining data from crops (Wood et al., 2017) and grassland (Verma et al., 2017) with a deciduous temperate forest, Sun et al. (2017) suggested a consistently strong SIF–GPP relationship across the three sites. Despite these encouraging results, the relationship between OCO-2 SIF and tower GPP has not yet been examined for other major biomes such as evergreen needleleaf forests, evergreen broadleaf forests, shrublands, and savannas due to the lack of OCO-2 overpasses and/or concurrent flux tower observations, and therefore it is also unclear whether there is a robust, consistent SIF–GPP relationship across a variety of biomes. A comprehensive analysis based on a large number of sites encompassing a wide variety of biomes will be timely and valuable for understanding the SIF–GPP relationships across biomes and will be essential for extensively using SIF observations from OCO-2 and future satellite missions in carbon cycle studies at regional to global scales.

Here we examined the relationship between OCO-2 SIF and tower GPP for a wide variety of biomes and assessed how the relationship varied among biomes using SIF and GPP data for a large number of flux sites across the globe. We identified and obtained data for a total of 64 EC flux sites over the globe after screening over 800 flux sites for the concurrent availability of OCO-2 and flux tower observations. With these observations, we examined the relationship between SIF and GPP for eight major biomes, and assessed to what extent the SIF–GPP relationship differed among biomes. To evaluate the performance of SIF for estimating GPP, we also assessed the relationship between MODIS-derived VIs and tower GPP. We elucidated the underlying causes for the strong SIF–GPP relationship by assessing how SIF and GPP were correlated with *f*PAR, APAR, and environmental stresses. Our study provides robust evidence for the value of OCO-2 SIF in estimating terrestrial photosynthesis for a wide variety of biomes, and demonstrates the great potential of OCO-2 SIF in ecosystem functioning and carbon cycling studies.

2 | MATERIALS AND METHODS

2.1 | Site description and flux tower data

We screened over 800 EC flux sites across the globe for the concurrent availability of OCO-2 SIF and flux tower observations over the period from September 2014 to present. For each EC site, we examined the availability of OCO-2 overpasses within the 5 km × 5 km area surrounding each tower. OCO-2 has sparse overpasses globally, which substantially limits the availability of OCO-2 soundings at flux sites (Figure 1a). For many EC flux sites, there were no OCO-2 overpasses within the 5 km × 5 km area surrounding the tower. For many of those towers having one or more OCO-2 overpasses, flux observations were not made during this period. For those sites having both OCO-2 and flux observations, we obtained flux data from the site principal investigators (PIs) for some of the sites; for some other sites, however, flux data were not shared with us at this stage. Eventually, we compiled a database consisting of a total of 64 EC flux tower sites having both OCO-2 and flux observations available since September 2014.

Figure 1 illustrates the OCO-2 overpasses and the location and distribution of the 64 EC flux tower sites. A more detailed description including site name, site code, location, biome types, and relevant references are summarized in Supporting information Table S1. The 64 sites encompass eight major biome types: evergreen needleleaf forests (14 sites), evergreen broadleaf forests (6 sites), deciduous broadleaf forests (4 sites), mixed forests (5 sites), open shrublands (9 sites), savannas (9 sites), grasslands (10 sites), and cropland (7 sites).

The EC technique continuously measures the net ecosystem exchange of carbon dioxide (NEE) between the ecosystem and the atmosphere at half-hourly or hourly time steps. The negative NEE values indicate ecosystem CO_2 uptake, and positive values indicate CO_2 release from the ecosystem to the atmosphere. The EC data analysis procedure includes data filtering (Papale et al., 2006) to reduce bias and to achieve high quality data and gap-filling. The data filtering leads to gaps in the data, mostly during nighttime when the friction velocity (u*) and the turbulent intensity are too low to allow a proper application of the EC method. The NEE measurements are routinely partitioned into GPP and ecosystem respiration (ER) using a nighttime partitioning approach (Reichstein et al., 2005). An empirical equation is

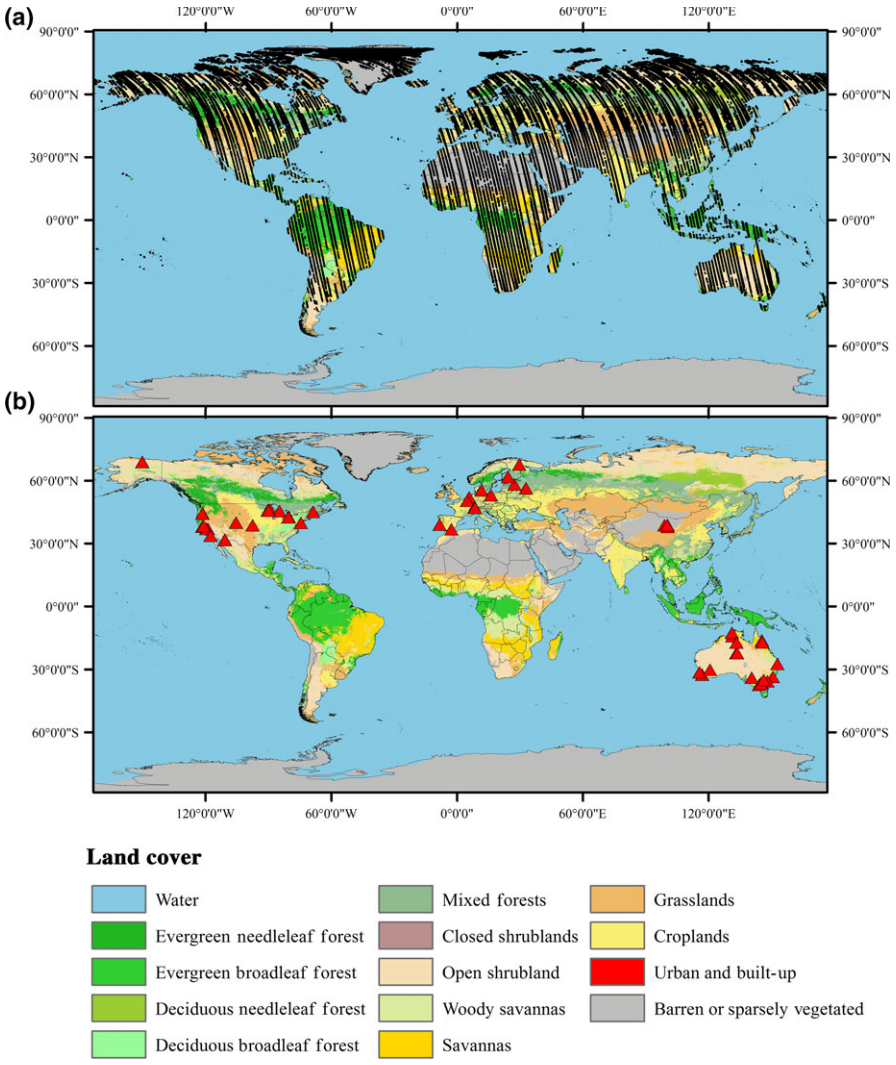

FIGURE 1 OCO-2 overpasses in July, 2015 (a) and the location and distribution of 64 EC flux sites across the globe (b). The triangles stand for EC flux sites. These sites were identified for concurrent availability of OCO-2 SIF and flux tower observations over the period from September 2014 to present after screening over 800 flux sites. The land cover map is from the MODIS Land Cover Type product (MCD12Q1) based on the University of Maryland (UMD) classification scheme [Colour figure can be viewed at wileyonlinelibrary.com]

developed between nighttime ER (i.e., nighttime NEE) and meteorological factors, and the equation is then used to estimate ER during the daytime; for each half-hourly or hourly time step, GPP is simply calculated as the difference between NEE and ER (Reichstein et al., 2005). A previous study applied 23 different partitioning methods to examine the effects of partitioning method choice on estimated GPP, and found that most methods differed by less than 10% in GPP estimates (Desai et al., 2008). Flux data based on daytime partitioning were also available for 10 out of the 64 sites. The daily GPP based on the nighttime partitioning was strongly correlated with that based on the daytime partitioning (Supporting information Figure S1; slope = 0.94, $R^2 = 0.89$, $p < 0.001$), showing that the use of daytime versus nighttime partitioning method had small effects on GPP estimates. For each of the 64 EC sites, we used tower GPP based on the nighttime partitioning method along with meteorological data (PAR, air temperature, vapor pressure deficit) in our analysis.

2.2 | OCO-2 SIF data

We obtained SIF data from the OCO-2 Lite products (V7r) from the OCO-2 data archive maintained at the NASA Goddard Earth Science Data and Information Services Center. The OCO-2 SIF data were produced by the OCO-2 project at the Jet Propulsion Laboratory. The OCO-2 SIF Lite files contain bias-corrected SIF along with other select fields aggregated as daily files. The OCO-2 spectrometer measures spectra in the O_2-A band, with far-red SIF retrieved at 757 and 771 nm based on the infilling of the Fraunhofer lines at 13:36 local time with data commencing on September 6, 2014 (Frankenberg et al., 2014). Typical OCO-2 measurements are collected alternately between nadir and glint viewing mode and a special target observation mode with a repeat frequency of approximately 16 days. The instrument views the ground directly below the spacecraft in the nadir mode, tracks near the location with direct sunlight reflected in the glint mode, and collects a large number of measurements over calibration/validation sites in the target mode (https://oco.jpl.nasa.gov).

For most of flux towers, the OCO-2 SIF retrievals were extracted within a distance of 2–5 km radius from the tower which is generally close to the size of the flux tower footprints. Because OCO-2's global coverage is extremely sparse, we used a larger radius (up to 25 km) to extract SIF for some relatively homogeneous sites (Supporting information Table S1) according to the MODIS land cover

map, which allowed us to increase the sample size of SIF retrievals at these sites. SIF retrievals of each site were estimated by taking the mean of all the soundings at which the grid cells had the same land cover type as the tower site. We conducted a sensitivity analysis to examine the effects of the varying radius (3, 5, 10, and 25 km) on SIF retrievals. OCO-2 provides SIF retrievals at two bands (751 and 771 nm, denoted as SIF_{757} and SIF_{771} henceforth) and two timescales (midday and daily).

2.3 | MODIS data

We also used MODIS-derived VIs: NDVI, EVI, and NIR_v in our analysis. Besides the three VIs, MODIS-derived *f*PAR and land cover datasets were also used in this study. MODIS land cover data were obtained from the NASA Land Processes Distributed Active Archive Center (LP DAAC), while other MODIS products were acquired from MODIS Collection 6 Land Products Global Subsetting and Visualization Tool.

NDVI and EVI are perhaps the most widely used VIs for monitoring vegetation conditions and estimating GPP (Dong et al., 2015; Sims et al., 2006; Sjöström et al., 2011; Xiao & Moody, 2005; Xiao et al., 2010). The newly proposed near-infrared reflectance of vegetation (NIR_v), the product of total scene NIR reflectance and NDVI, has been shown to be better related to GPP than NDVI or NIR alone (Badgley, Field, & Berry, 2017). These three VIs were derived from two MODIS products: Terra reflectance products (MOD09A1, 8-day, 500 m) and bidirectional reflectance distribution function (BRDF) corrected reflectance products (MCD43A4, daily, 500 m). For temperate forests, the BRDF-corrected NDVI and EVI, $NDVI_{BRDF}$ and EVI_{BRDF}, were more strongly related to tower GPP than were NDVI and EVI, respectively; EVI_{BRDF} had the strongest correlation with GPP among these four VIs (Li et al., 2018a). *f*PAR was obtained from the combined MODIS product (MCD15A3H, 4-day, 500 m). The land cover data were based on the MODIS Land Cover Type product (MCD12Q1) with the University of Maryland (UMD) land cover classification scheme.

2.4 | Analysis

The relationship between OCO-2 SIF and tower GPP was evaluated for both SIF retrieval bands (SIF_{757} and SIF_{771}) and two timescales (midday and daily) using OCO-2 and tower data for the 64 EC sites encompassing eight biomes. The instantaneous (1:30 p.m. or midday) SIF was evaluated against midday tower GPP. Almost all the flux sites provided half-hourly GPP data, and the midday tower GPP was calculated as the averaged GPP for two half-hours: 1:00–1:30 p.m. and 1:30–2:00 p.m. For one site, EE-Jvs, the GPP at 1:15–1:45 p.m. was considered as the midday tower GPP. Two sites (AU-Tum and US-PFa) provided hourly GPP data, and the hourly values during the interval 1:00–2:00 p.m. were considered as the midday tower GPP. To evaluate the SIF–GPP relationship at the daily timescale, the midday SIF retrievals were converted to daily SIF by applying the daily correction factor provided in the OCO-2 SIF Lite product. The different measurement modes (nadir, glint, and target) have different viewing zenith angles. To examine whether the changing viewing geometries affect the interpretation of SIF data and the SIF–GPP relationship, we examined whether SIF averaged from measurement modes is statistically different using the one-way Analysis of Variance (ANOVA) method and compared the statistical differences in the slope of the resulting SIF–GPP relationships using a two-tailed *t* test. Due to the low number of SIF retrievals collected in the target mode, the soundings in the target and glint mode were pooled together to compare with those in the nadir mode. To help assess the value of OCO-2 SIF in estimating GPP, we examined the relationships between GPP and three VIs including NDVI, EVI, and NIR_v derived from two MODIS products. Unlike SIF, VIs do not contain information on instantaneous radiation or PAR. Therefore, the relationships between tower GPP and VIs × PAR were also evaluated for a fair comparison between VIs and SIF. The daily VIs for those days having OCO-2 SIF were used in the analysis. The corresponding daily Terra VIs were interpolated from the original 8-day products and were then compared with tower GPP.

Previous research based on GOSAT or GOME-2 SIF showed that the relationship between satellite-derived SIF and gridded GPP data varied across biomes (Guanter et al., 2012; Parazoo et al., 2014; Zhang et al., 2016). Our comparison using global flux data enables us to investigate whether this conclusion also holds for OCO-2 SIF and tower GPP and whether the strong SIF–GPP relationship is consistent across a wide variety of biomes at the ecosystem scale. A biome-specific SIF–GPP relationship was fitted for each biome, and the differences in the slopes of the derived SIF–GPP relationships between any two biomes were then examined by a two-tailed *t* test. In addition, we also examined whether C_3 and C_4 species shared the same SIF–GPP relationship because two previous studies showed C_4 crops had a higher SIF–GPP slope than C_3 crops (Liu, Guan, & Liu, 2017; Wood et al., 2017). The SIF–GPP relationship was examined for grasslands/croplands dominated by C_3 and C_4 species separately, and the difference in the slopes was then examined by a two-tailed *t*-test.

We also analyzed the relationship between SIF and *f*PAR, APAR (*f*PAR × tower PAR) and two environmental scalars, *f*Tmin and *f*VPD, representing low temperature and high vapor pressure deficit (VPD) stresses, respectively, to reveal how SIF responds to these factors. Temperature is one of the most important abiotic factors regulating plant photosynthesis. Low temperature imposes a limit on the activity of enzymes and effective maximum rate of carboxylation (V_{cmax}) in the photosynthesis processes, and therefore decreases the capacity and efficiency of photosynthesis (Öquist, 1983). VPD is an effective measure of atmospheric water stress. High VPD mainly inhibits photosynthesis by reducing leaf stomatal conductance and intercellular CO_2 concentration (Dai, Edwards, & Ku, 1992). As the VPD increases, the drying ability of air increases. In this case, plants need to draw more water from the roots in an effort to avoid wilting (Tardieu, 2013). *f*Tmin and *f*VPD were calculated based on the MODIS GPP algorithm (Running et al., 2004) using flux tower meteorological measurements.

We chose two flux tower sites with a larger number of temporal OCO-2 overpasses, Hyytiälä forest (FI-Hyy, 23 daily SIF observations) and Daly River Savanna (AU-Das, 19 daily SIF observations), to examine how variations in GPP and SIF were determined by changes in the APAR and two environmental factors. The chosen sites have different environmental controls on photosynthesis. FI-Hyy is located in a boreal evergreen forest with an annual mean temperature of about 3°C. Air temperature is more important in regulating photosynthesis than water availability at the FI-Hyy site (Mäkelä et al., 2006). AU-Das is classified as a tropical woodland savanna that is not temperature limited and has seasonal water limitation during the dry season (Rogers & Beringer, 2017). Therefore, water availability may have a larger effect on photosynthesis at the AU-Das site. We expected that SIF would respond in a similar way to the temperature and water stresses (*f*Tmin and *f*VPD) as GPP, which if true would further support a strong SIF–GPP relationship.

Finally, we conducted twofold evaluations on the performance of OCO-2 SIF for GPP estimation. Four EC flux sites covering different biomes were first selected to compare the performance of the SIF–GPP linear model for estimating GPP with that of the GPP-EVI linear model and the MODIS GPP algorithm (Equation 3).

$$GPP = \epsilon_{max} \times PAR \times fPAR \times fT_{min} \times fVPD \quad (3)$$

where ε_{max} is the biome-dependent maximum LUE_p.

We examined whether SIF has consistent superiority over MODIS-derived VIs and the LUE model in GPP estimation across biomes. These sites have a larger number of temporal SIF retrievals, including FI-Hyy (ENF), AU-Das (SAV), Arou (GRA, 25 daily SIF observations), and Daman (CRO, 20 daily SIF observations). For the SIF-GPP linear model, the universal SIF–GPP relationship (derived from all the observations for all the sites/biomes) and biome-specific SIF–GPP relationships were both applied. We then carried out K-fold cross-validation using all the observations to assess the predictive ability of SIF and EVI in estimating GPP. The simulations were performed 20 times, and the average value was taken as fitted GPP. Their performance of the SIF–GPP linear model was also compared with that the MODIS GPP algorithm. The comparative performance was evaluated by coefficient of determination (R^2) and Root Mean Square Error (RMSE).

3 | RESULTS

3.1 | Relationships of OCO-2 SIF and MODIS VIs with tower GPP

The OCO-2 SIF showed overall a strong linear correlation with tower GPP regardless of retrieval bands and timescales (Figure 2). In general, the goodness-of-fit was better for the daily timescale (SIF_{757}: $R^2 = 0.72$, $p < 0.0001$; SIF_{771}: $R^2 = 0.55$, $p < 0.0001$) than for the midday (or instantaneous) timescale (SIF_{757}: $R^2 = 0.62$, $p < 0.0001$; SIF_{771}: $R^2 = 0.48$, $p < 0.0001$), and SIF_{757} was more strongly correlated with tower GPP than was SIF_{771} at both timescales. The strongest relationship was observed for SIF_{757} at the daily timescale ($R^2 = 0.72$, $p < 0.0001$). We also examined the relationships of tower GPP and the SIF averaged from SIF_{757} and SIF_{771} (multiplying SIF_{771} by 1.5), and found that the averaged SIF (daily: $R^2 = 0.68$, $p < 0.0001$; midday: $R^2 = 0.59$, $p < 0.0001$) exhibited

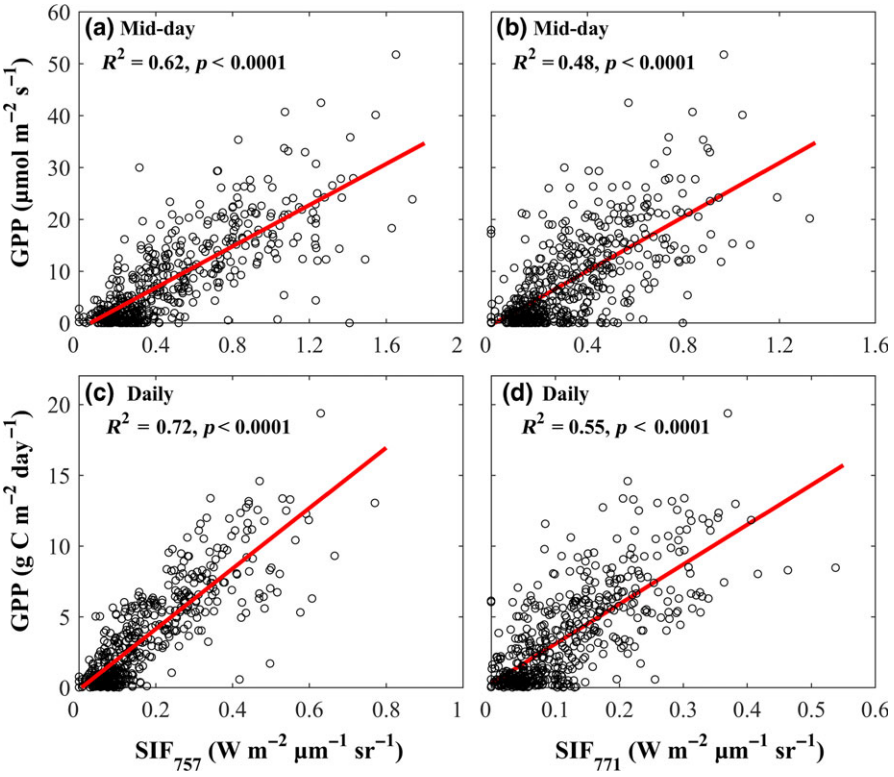

FIGURE 2 The relationships between tower GPP and OCO-2 SIF at 64 flux tower sites encompassing eight major biomes. (a) GPP vs. SIF_{757} at the midday (or instantaneous) timescale ($GPP = 19.97 \times SIF_{757} - 1.17$); (b) GPP vs. SIF_{771} at the midday (or instantaneous) timescale ($GPP = 26.16 \times SIF_{771} - 0.38$); (c) GPP vs. SIF_{757} at the daily timescale ($GPP = 21.38 \times SIF_{757} - 0.14$); (d) GPP vs. SIF_{771} at the daily timescale ($GPP = 28.04 \times SIF_{771} + 0.28$) [Colour figure can be viewed at wileyonlinelibrary.com]

stronger correlation with tower GPP than SIF_{771} but slightly weaker correlation than SIF_{757} (Supporting information Figure S2). For the 10 sites also having GPP estimates based on the daytime partitioning method, we examined the effects of nighttime versus daytime partitioning on the SIF–GPP relationship, and the resulting two slopes were not significantly different from each other (Supporting information Figure S3).

There was no significant difference in the mean SIF between the nadir mode (305 observations) and the glint (or target) mode (211 observations) for both midday (ANOVA: $p = 0.09$) and daily timescales (ANOVA: $p = 0.51$) (Figure 3a,b). Consequently, the SIF–GPP relationship did not significantly vary with the measurement mode at both midday and daily timescales (Figure 3c,d). SIF in the nadir mode exhibited a slightly stronger relationship with tower GPP than that in the glint/target mode at the midday timescale but a similarly strong relationship with GPP as that in the glint/target mode at the daily timescale (Table 1). The difference in the slope of the SIF–GPP relationship was not statistically significant between the two measurement modes for both retrieval bands and timescales ($p > 0.05$) except for SIF_{771} at the daily timescale ($p = 0.02$), suggesting that the modes (or viewing zenith angles) generally had no significant effects on the SIF–GPP relationships. For SIF_{757} at the daily timescale, the slope of the SIF–GPP relationship based on data from both modes was not significantly different from that based on data from either nadir or glint/target mode. Only SIF_{757} was used hereafter due to its stronger correlation with tower GPP relative to SIF_{771}. In the following analyses, we did not separate modes in order to increase the number of observations because the measurements modes did not significantly affect the SIF–GPP relationship for SIF_{757}.

Our sensitivity analysis showed the extracting radius of SIF soundings had no significant effects on the interpretation of the SIF–GPP relationship (Supporting information Figure S4). The corresponding slopes were similar to each other (18.83 to 21.07 g C m^{-2} day^{-1}/W m^{-2} μm^{-1} sr^{-1}) and did not significantly differ ($p > 0.1$, two-tailed t test), which indicated that the relationship was relatively stable across these scales. The R^2 value of the relationship between SIF and GPP increased from 0.64 to 0.71 with the radius increasing from 3 to 25 km, indicating that spatial averaging smoothed out the spatial variability and improved the SIF–GPP relationship.

The three VIs (NDVI, EVI, and NIR_v) derived from two MODIS products were also strongly correlated with tower GPP (Terra: $R^2 = 0.55$–0.62, $p < 0.0001$; BRDF corrected: $R^2 = 0.60$–0.65, $p < 0.0001$) (Figure 4). The products of VIs and PAR (VIs × PAR) showed similar correlations with tower GPP (Terra: $R^2 = 0.50$–0.59, $p < 0.0001$; BRDF corrected: $R^2 = 0.61$–0.63, $p < 0.0001$) (Supporting information Figure S5) as VIs alone. The BRDF-corrected VIs showed slightly stronger correlation with tower GPP than the Terra vegetation indices (Figure 4). EVI and NIR_v had slightly stronger correlation with tower GPP than NDVI. Nevertheless, the strongest relationship between tower GPP and MODIS-derived VIs (EVI_{BRDF}: $R^2 = 0.64$, $p < 0.0001$; BRDF-corrected NIR_v: $R^2 = 0.65$, $p < 0.0001$) was slightly weaker than the relationship between tower GPP and OCO-2 SIF_{757} ($R^2 = 0.71$, $p < 0.0001$).

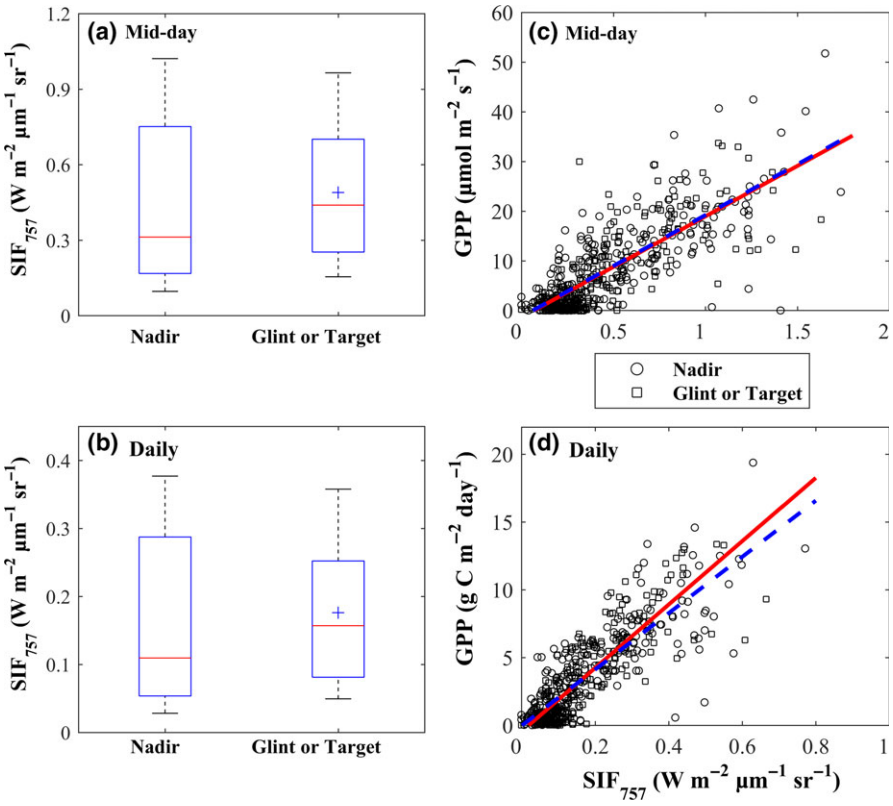

FIGURE 3 The distributions of OCO-2 SIF_{757} (a) at the midday timescale and (b) at the daily timescale and the corresponding relationship between OCO-2 SIF_{757} and tower GPP (c) at the midday timescale and (d) at the daily timescale for both nadir and glint (or target) modes. OCO-2 SIF data collected in different modes were fitted by different lines, with the blue dashed line for the nadir mode, and the red solid line for the glint (or target) mode. The slopes and intercepts of the regression models are summarized in Table 1 [Colour figure can be viewed at wileyonlinelibrary.com]

TABLE 1 Statistical measures for the relationships between tower GPP and OCO-2 SIF

		Both modes			Nadir mode			Glint (or target) mode		
Timescale	Band (nm)	Slope	Intercept	R^2	Slope	Intercept	R^2	Slope	Intercept	R^2
Midday	757	19.97	−1.17	0.62	19.79	−1.06	0.65	20.28	−1.38	0.58
Midday	771	26.16	−0.38	0.48	26.42	−0.17	0.49	25.93	−0.84	0.43
Daily	757	21.38	−0.14	0.72	20.35	0	0.73	23.37	−0.45	0.71
Daily	771	28.04	0.28	0.55	26.61	0.51	0.55	31.11	−0.23	0.58

Note: All the correlations were statistically significant ($p < 0.0001$). In the regression models, the units of GPP at the midday and daily timescales are μmol m^{-2} s^{-1} and g C m^{-2} day^{-1}, respectively; the units of SIF are W m^{-2} μm^{-1} sr^{-1}.

Among the 64 flux sites, some sites had a larger number of overpasses and these sites may have larger influences on the resulting SIF–GPP relationship. Therefore, we also evaluated the SIF–GPP and EVI_{BRDF}–GPP relationships at the site level by averaging SIF, EVI_{BRDF}, and GPP for each site, respectively (Figure 5). We found that both SIF–GPP and EVI_{BRDF}–GPP relationships were strong at the site level, with the SIF–GPP relationship ($R^2 = 0.77$, $p < 0.0001$) slightly stronger than the EVI_{BRDF}–GPP relationship ($R^2 = 0.67$, $p < 0.0001$). The $EVI_{BRDF} \times PAR$ had a slightly weaker correlation with tower GPP ($R^2 = 0.51$, $p < 0.0001$), and the use of two scalars (fT_{min} and $fVPD$) improved the relationship ($R^2 = 0.68$, $p < 0.0001$) (Supporting information Figure S6).

3.2 | Biome-specific SIF–GPP relationships

We examined the relationship between OCO-2 SIF and tower GPP for each biome (Figure 6), and found a consistently strong relationship between GPP and SIF for all eight biomes ($R^2 = 0.57$–0.79, $p < 0.0001$) except evergreen broadleaf forests ($R^2 = 0.16$, $p < 0.05$). The slope was the greatest for grasslands (25.43 g C m^{-2} day^{-1}/W m^{-2} μm^{-1} sr^{-1}) and the smallest for evergreen broadleaf forests (6.30 g C m^{-2} day^{-1}/W m^{-2} μm^{-1} sr^{-1}). The remaining six biomes had very similar slopes: 21.19 (evergreen needleleaf forests), 20.01 (deciduous broadleaf forests), 19.92 (mixed forests), 22.07 (open shrublands), 19.04 (savannas), and 20.29 g C m^{-2} day^{-1}/W m^{-2} μm^{-1} sr^{-1} (croplands). The slope of the SIF-GPP relationship for most biomes was not significantly different from slopes for other biomes (Supporting information Table S2). Only the relationship for grasslands was significantly different from that for evergreen needleleaf forests, mixed forests, savannas, and croplands. C_4-dominated grasslands and crops had a significantly higher slope than C_3-dominated grasslands and crops (29.42 g C m^{-2} day^{-1}/W m^{-2} μm^{-1} sr^{-1} vs. 20.98 g C m^{-2} day^{-1}/W m^{-2} μm^{-1} sr^{-1}, $p < 0.0001$, Figure 7). The relationships between EVI_{BRDF} and GPP were strong for all biomes except evergreen broadleaf forests (Supporting information Figure S7). SIF exhibited stronger correlation with GPP than did EVI_{BRDF}, for open shrublands, grasslands, and croplands, while EVI_{BRDF} had stronger correlation with GPP than did SIF for deciduous broadleaf forests, mixed forests, and savannas (Figure 6, Supporting information Figure S7).

The mean SIF and GPP values varied with biome (Figure 8a). The one-way ANOVA test results for the differences in SIF and GPP among biomes are provided in Supporting information Table S3. Evergreen broadleaf forests and deciduous broadleaf forests had the highest mean SIF and GPP; evergreen needleleaf forests, mixed forests, and croplands had intermediate values, followed by savannas, open shrublands, and grasslands had the lowest values. The biome averaged SIF was highly correlated with averaged GPP across the eight biomes ($R^2 = 0.95$, $p < 0.0001$, Figure 8b), demonstrating the potential of OCO-2 SIF in GPP estimation across a wide variety of biomes.

3.3 | Relationships of OCO-2 SIF with APAR and environmental stresses

Our results showed that APAR explained 60% of the variance in SIF, indicating that SIF mainly depended on APAR. The product of APAR with two environmental scaling factors ($APAR \times fT_{min} \times fVPD$) explained higher variance in SIF_{757} ($R^2 = 0.70$, $p < 0.0001$) than $fPAR$ ($R^2 = 0.57$, $p < 0.0001$) or APAR ($R^2 = 0.60$, $p < 0.0001$) alone (Figure 9). This indicates that SIF was mainly driven by APAR and was also influenced by environmental stresses, which explained why there was a strong relationship between GPP and SIF. These two environmental scalars also impacted photosynthesis, specifically LUE_p. Therefore, SIF was also associated with LUE_p. EVI_{BRDF} had a much stronger relationship with $fPAR$ than with APAR, indicating that EVI_{BRDF} is mainly a proxy for $fPAR$ and may not contain information on PAR; EVI_{BRDF} also contained information on environmental stresses (Figure 9).

The seasonal cycles of OCO-2 SIF, flux tower GPP, two environmental scalars ($fTmin$ and $fVPD$), and APAR at the FI-Hyy site are shown in Figure 10. Here, APAR and $fTmin$ explained 41% and 45% of the variance in SIF, respectively, while the product of APAR and $fTmin$ explained much higher variance in SIF ($R^2 = 0.61$, $p < 0.0001$). VPD is not a dominant controlling factor on photosynthesis in the FI-Hyy boreal ecosystem, and it was not directly correlated with SIF ($p > 0.05$). $APAR \times fTmin \times fVPD$ explained slightly higher variance in SIF ($R^2 = 0.65$, $p < 0.0001$) than $APAR \times fTmin$. Similar conclusions also hold for tower GPP at this site. Tower GPP was largely influenced by $APAR \times fTmin$ ($R^2 = 0.76$, $p < 0.0001$). $APAR \times fTmin \times fVPD$ explained the same variance in GPP ($R^2 = 0.76$, $p < 0.0001$) as $APAR \times fTmin$, showing that VPD had negligible contribution to GPP. At the AU-Das savanna site (Figure 11), APAR also explained much of the

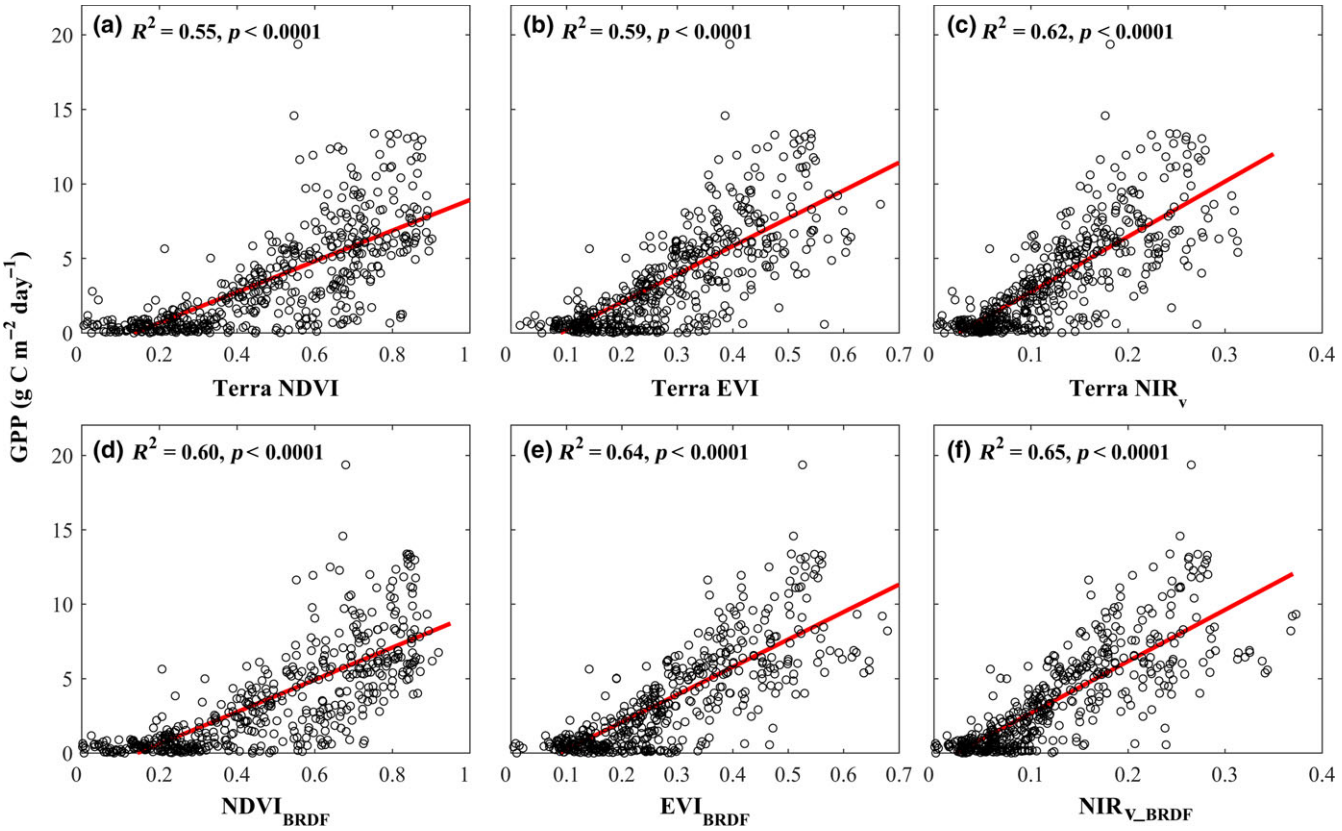

FIGURE 4 Relationships between tower GPP and VIs (NDVI, EVI, and NIR_v) derived from two MODIS reflectance products: (a–c) MOD09A1 (Terra) and (d–f) MCD43A4 (BRDF corrected) [Colour figure can be viewed at wileyonlinelibrary.com]

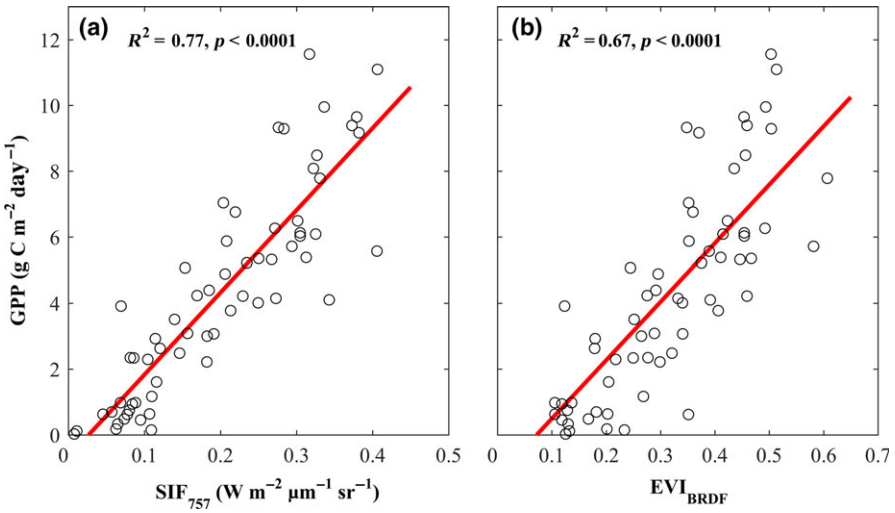

FIGURE 5 The relationships of OCO-2 SIF and MODIS-derived EVI with tower GPP at the site level across the 64 eddy covariance flux sites over the globe: (a) SIF versus GPP; (b) EVI_{BRDF} versus GPP. For each site, SIF, EVI_{BRDF}, and GPP were averaged over all days, respectively [Colour figure can be viewed at wileyonlinelibrary.com]

seasonal variation in SIF ($R^2 = 0.60$, $p < 0.0001$). However, SIF was not affected by *f*Tmin at AU-Das; APAR × *f*VPD was more strongly related to SIF ($R^2 = 0.66$, $p < 0.0001$) than APAR alone. Similarly, GPP also largely depended on APAR ($R^2 = 0.60$, $p < 0.0001$) and *f*VPD ($R^2 = 0.38$, $p < 0.0001$). For this Australian savanna site, temperature is not a limiting factor, whereas VPD is an important controlling factor on GPP. Although the environmental controls on photosynthesis at these two sites were different, SIF responded to the environmental stresses in a similar way as GPP.

3.4 | Evaluating the performance of the SIF–GPP linear relationship for estimating GPP

We evaluated the performance of the SIF–GPP linear relationship derived from OCO-2 SIF_{757} and flux tower GPP for estimating GPP

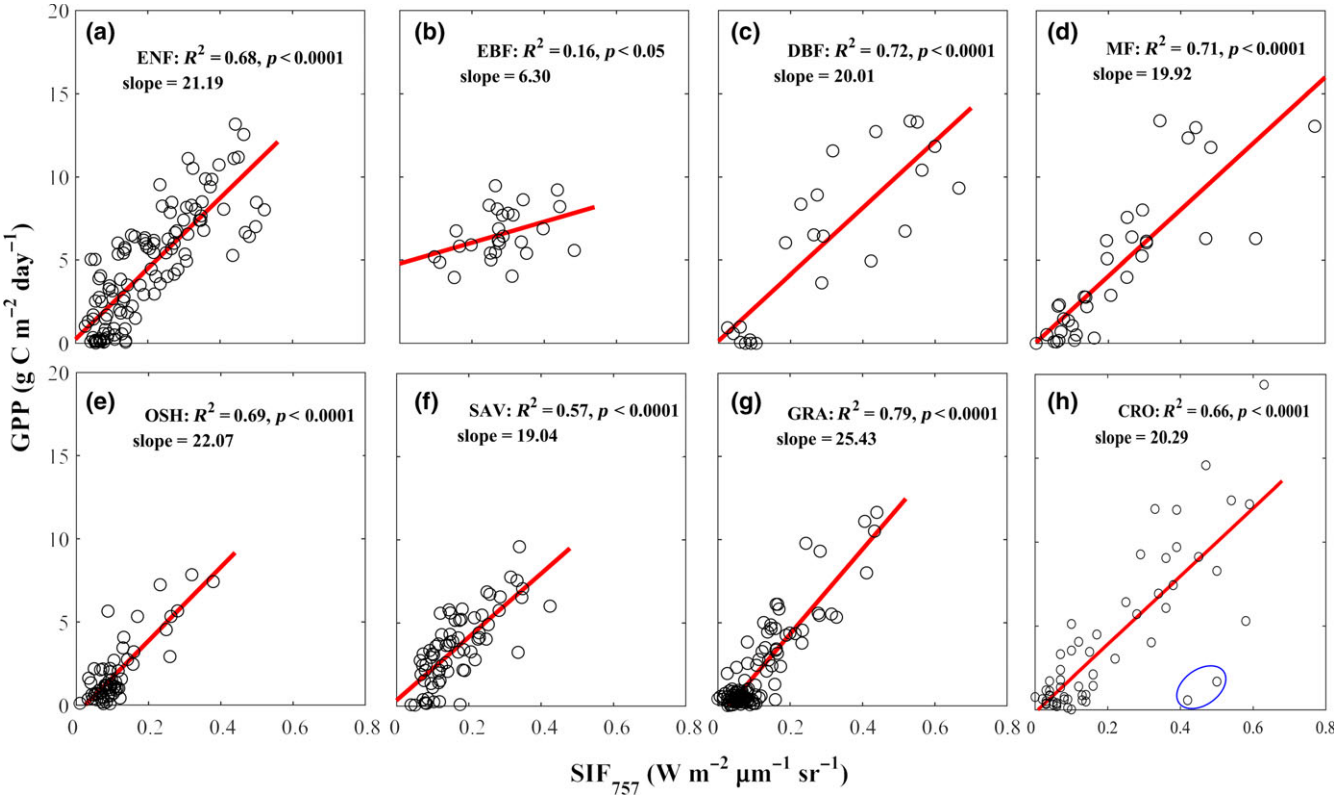

FIGURE 6 Scatter plots of daily tower GPP and OCO-2 SIF for individual biomes: (a) evergreen needleleaf forests (ENF); (b) evergreen broadleaf forests (EBF); (c) deciduous broadleaf forests (DBF); (d) mixed forests (MF); (e) open shrublands (OSH); (f) savannas (SAV); (g) grasslands (GRA); (h) croplands (CRO). The solid lines represent the fitted regression lines. The relationship between SIF and GPP for croplands was stronger (R^2 = 0.79, p < 0.0001) when the two outliers highlighted by the blue circle were removed [Colour figure can be viewed at wileyonlinelibrary.com]

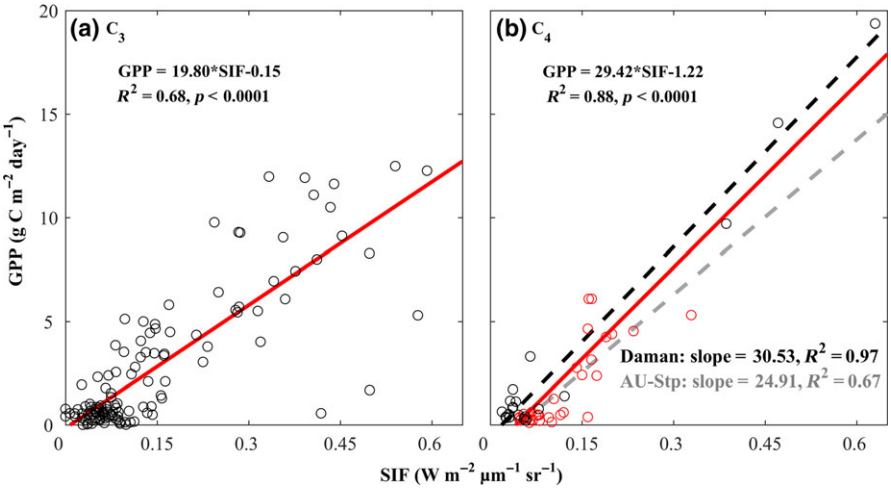

FIGURE 7 Scatter plots of daily tower GPP and OCO-2 SIF for C3 (a) and C4 (b) grasslands and croplands. The SIF–GPP relationships in C_4 vegetation were examined at both Daman and AU-Stp sites. The red solid lines represent the fitted regression lines. The black and gray dashed lines in (b) are regression lines for the Daman and Au-Stp sites, respectively [Colour figure can be viewed at wileyonlinelibrary.com]

at four selected flux sites covering different biomes, and also used MODIS-derived EVI_{BRDF} and a LUE model (the MODIS GPP algorithm) to estimate GPP for comparison purposes (Figure 12). In general, GPP estimates based on the universal SIF–GPP relationship had high consistency with tower GPP, with R^2 values ranging from 0.80 to 0.96 and RMSE from 1.05 to 2.10 g C m^{-2} day^{-1}. Applying biome-specific SIF–GPP relationships (R^2 = 0.80–0.96, RMSE = 1.00–2.17 g C m^{-2} day^{-1}) showed very similar performance to the universal relationship. The EVI_{BRDF}-based model performed as well as the SIF-based model in predicting GPP of the four selected sites (R^2 = 0.65 for AU-Das and 0.90–0.91 for other three sites, RMSE = 0.65–2.96 g C m^{-2} day^{-1}). In addition, GPP estimates from SIF and EVI_{BRDF} tracked the seasonality in tower GPP well, especially SIF at FI-Hyy and Arou and EVI_{BRDF} at AU-Das. The MODIS GPP model overall had a slightly lower performance at these sites (R^2 = 0.69–0.96, RMSE = 2.31–4.2 g C m^{-2} day^{-1}), and it largely

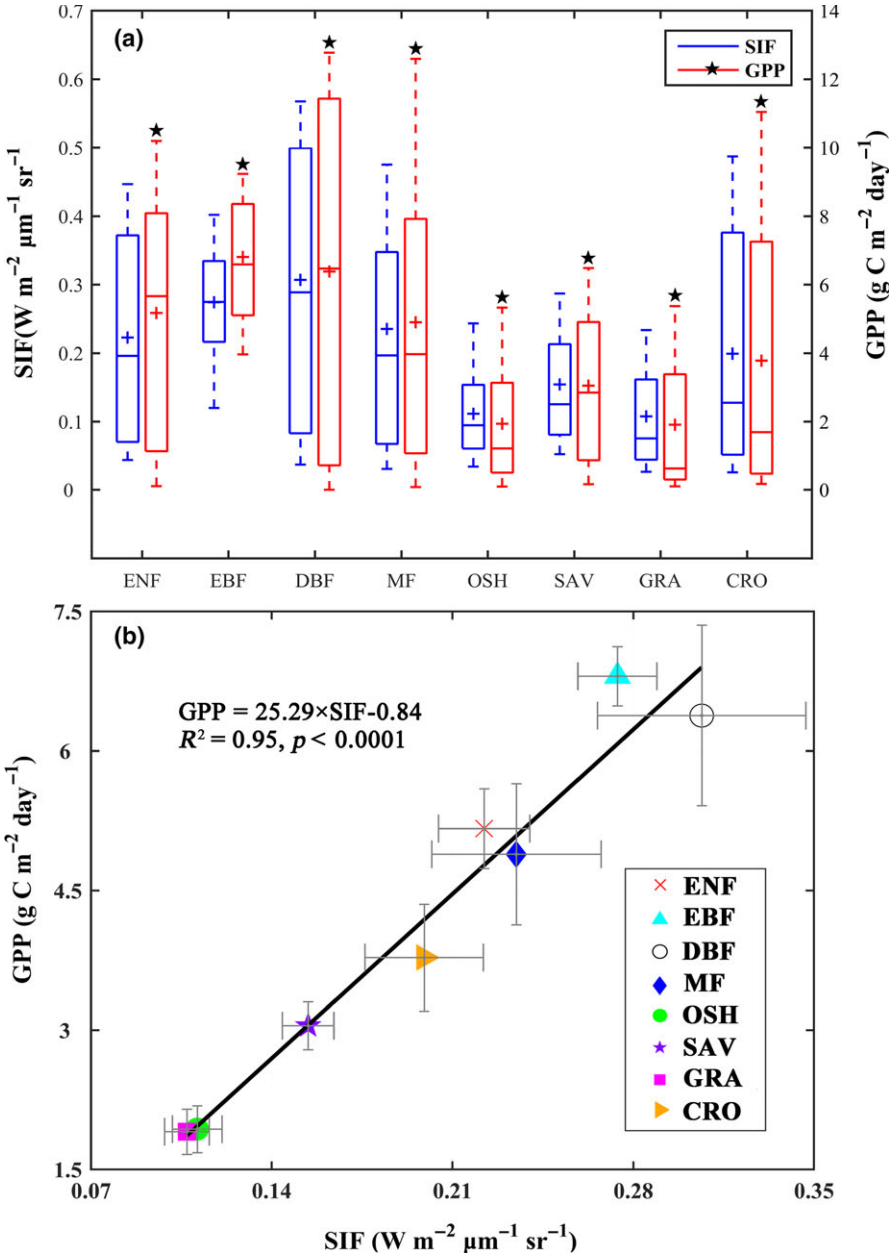

FIGURE 8 The boxplots of OCO-2 SIF_{757} and tower GPP for each biome and the GPP–SIF relationship at the biome level. The boxplots (a) display the distributions of SIF and tower GPP for eight major biomes. (b) shows the biome averaged SIF and GPP relationship with error bars for the standard deviations across all sites in the biome [Colour figure can be viewed at wileyonlinelibrary.com]

underestimated GPP at higher magnitudes of GPP (GPP > 5 g C m^{-2} day^{-1}).

We also evaluated the performance of SIF and EVI_{BRDF} for estimating GPP using cross-validation, and then compared these estimates to those of the MODIS GPP algorithm (Figure 13). Overall, all the methods estimated GPP fairly well. The GPP estimates based on SIF (R^2 = 0.71, p < 0.0001, RMSE = 1.80 g C m^{-2} day^{-1}) were more strongly correlated with tower GPP and had lower RMSE than those based on EVI_{BRDF} (R^2 = 0.64, p < 0.0001, RMSE = 2.02 g C m^{-2} day^{-1}) or the MODIS GPP algorithm (R^2 = 0.66, p < 0.0001, RMSE = 2.23 g C m^{-2} day^{-1}). This shows that the universal SIF–GPP relationship could estimate GPP slightly better than vegetation indices and the light use efficiency model.

4 | DISCUSSION

Using the concurrent OCO-2 SIF and flux tower observations (2014–2017) from a total of 64 EC flux sites encompassing eight major biomes across the globe, we found that the OCO-2 SIF showed strong linear correlation with tower GPP in different retrieval bands (757 and 771 nm), timescales (midday and daily), and measurement modes (nadir and glint/target). The measurements modes had no significant effects on the slope of the SIF–GPP relationship for both retrieval bands and timescales except for SIF_{771} at the daily timescale. The strong relationships between SIF_{757} and GPP at the ecosystem scale were found consistently in seven out of the eight biomes, which supports and substantially expands the findings of the pioneering studies on OCO-2 SIF (Li et al., 2018a; Sun et al., 2017;

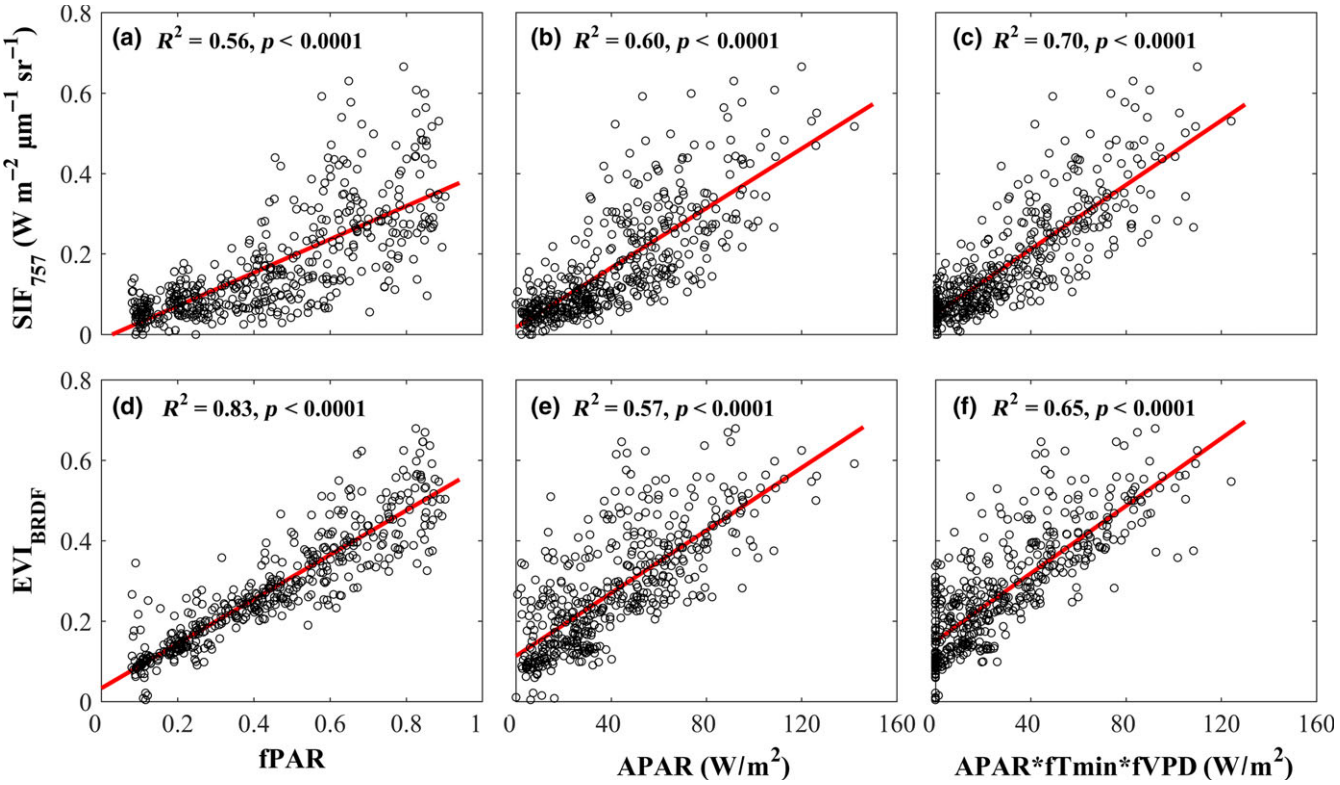

FIGURE 9 Relationships of OCO-2 SIF and EVI_{BRDF} with *f*PAR, APAR, and the product of APAR with two environmental scalars: (a) SIF versus *f*PAR; (b) SIF versus APAR; (c) SIF versus APAR × *f*Tmin × *f*VPD; (d) EVI_{BRDF} versus fPAR; (e) EVI_{BRDF} versus APAR; (f) EVI_{BRDF} versus APAR × *f*Tmin × *f*VPD [Colour figure can be viewed at wileyonlinelibrary.com]

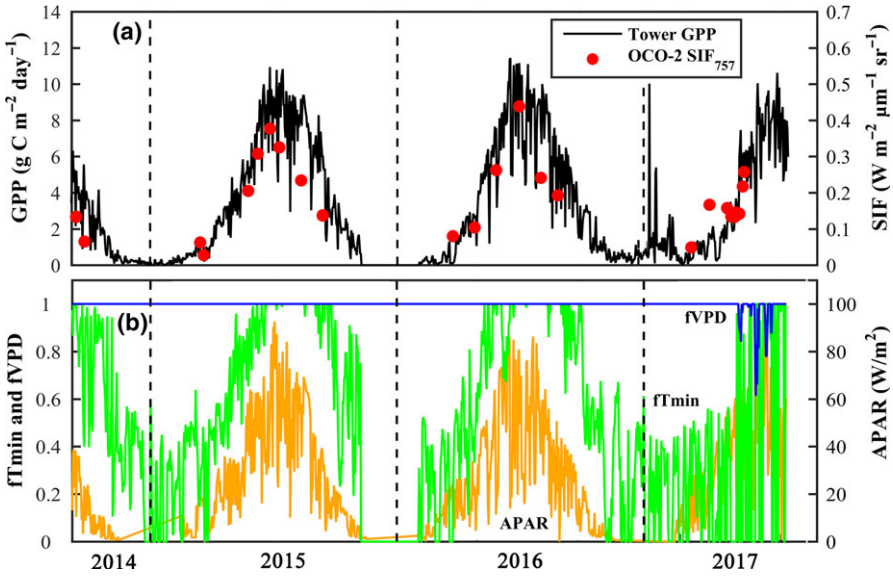

FIGURE 10 The seasonal cycles of OCO-2 SIF, flux tower GPP, two environmental scalars (*f*Tmin and *f*VPD), and APAR at the Hyytiälä forest (FI-Hyy, Finland) from September 6, 2014 to July 31, 2017: (a) SIF and GPP; (b) environmental scalars and APAR [Colour figure can be viewed at wileyonlinelibrary.com]

Verma et al., 2017; Wood et al., 2017). They reported slightly stronger relationships between OCO-2 SIF and tower GPP in temperate forests, grassland, and crops. Our results demonstrated that OCO-2 SIF was also strongly related to tower GPP for other biomes: evergreen needleleaf forests, open shrublands, and savannas. The weak linear relationship that we found for evergreen broadleaf forests may have resulted from several factors. First, it is challenging for satellite measurements to detect the canopy activity of tropical forests. On one hand, the satellite measurements may not detect all of the activity (understory, midcanopy located plants, and the very large and dense canopy) (Tang & Dubayah, 2017). On the other hand, satellite-based indicators are sensitive to atmospheric cloud/aerosol contamination or sun–sensor geometry which can confound the real seasonality of forests, although the SIF is considered to be less sensitive than various VIs (Frankenberg et al., 2014). Second, the ongoing challenges and large uncertainty in estimating GPP in

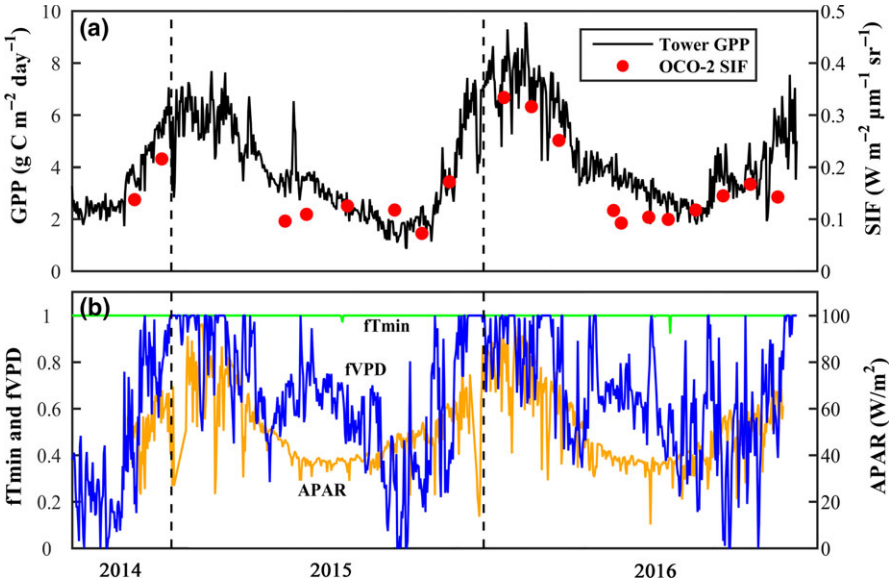

FIGURE 11 The seasonal cycles of OCO-2 SIF, flux tower GPP, two environmental scalars (*f*Tmin and *f*VPD), and APAR at the Daly River Savanna site (AU-Das, Australia) from September 6, 2014 to December 31, 2016: (a) SIF and GPP; (b) environmental scalars and APAR [Colour figure can be viewed at wileyonlinelibrary.com]

tropical forests using the eddy covariance technique could also lead to the weaker SIF–GPP relationship (Hayek et al., 2018). Third, the very limited number of OCO-2 soundings only captured a part of the seasonal variations in SIF and GPP. The tower GPP in evergreen broadleaf forests for those days having OCO-2 soundings only ranged from 5–10 g C m^{-2} day^{-1}, and the range was indeed much smaller than that in evergreen needleleaf forests, deciduous broadleaf forests, and mixed forests (all between roughly 0 and 13 g C m^{-2} day^{-1}). It was reasonable to assume that the relationship in evergreen broadleaf forests might be largely improved should more SIF observations with the corresponding GPP beyond the small range (5–10 g C m^{-2} day^{-1}) be available. Previous research based on either GOSAT (Guanter et al., 2012) or GOME-2 SIF (Madani, Kimball, Jones, Parazoo, & Guan, 2017; Zhang et al., 2016) also reported weaker SIF–GPP relationships in evergreen broadleaf forests, which may also be caused by one or more of the factors described above.

Our global analysis showed that the SIF–GPP relationship based on OCO-2 SIF_{757} and tower GPP was similar among biomes, and the slopes in most of the biomes were not significantly different from each other. This finding is an important distinction and simplification compared to previous results based on coarser-resolution SIF data and gridded GPP data products (Guanter et al., 2012; Parazoo et al., 2014). The previous assumption of biome-specific SIF–GPP relationships seems reasonable because the SIF–GPP relationship results from multiple factors such as difference in plant physiology and canopy structure, environmental conditions, changes in surface illumination, and different contributions from photosystem I and II, which may be naturally different across biomes (Damm et al., 2015; Porcar-Castell et al., 2014; Sun et al., 2017). The SIF–GPP relationship was mainly dominated by APAR and also affected by the covariations in LUEp and Θ_f (Equations 1 and 2). Both LUEp and Θ_f vary with environmental conditions (e.g., light, water, atmospheric CO_2) and could be positively correlated with each other (Yang et al., 2015, 2016). Therefore, should a universal SIF–GPP linear relationship exist, at least the variations in LUE_p and Θ_f among biomes should offset each other (Sun et al., 2017). The highly biome-dependent SIF–GPP relationships reported previously may partly result from the systematic biases in gridded GPP datasets (Sun et al., 2018). Sun et al. (2017) found similar values of slope in crops (16.06 g C m^{-2} day^{-1}/W m^{-2} μm^{-1} sr^{-1}), forest (15.31 g C m^{-2} day^{-1}/W m^{-2} μm^{-1} sr^{-1}), and grass (16.37 g C m^{-2} day^{-1}/W m^{-2} μm^{-1} sr^{-1}) using OCO-2 SIF and tower GPP. However, only three biomes and a very limited number of observations (~30) were involved in this previous study. Our global analysis based on a total of 64 sites across the globe revealed a nearly universal SIF–GPP relationship across a wide variety of biomes for the first time. The only exceptions lie in the weak relationship for evergreen broadleaf forests and the higher slope of grasslands (25.43 g C m^{-2} day^{-1}/W m^{-2} μm^{-1} sr^{-1}) relative to the universal slope (21.38 g C m^{-2} day^{-1}/W m^{-2} μm^{-1} sr^{-1}). Currently, there is no evidence that the mechanism coupling the fluorescence and photosynthesis in grasslands is different from other biomes. The higher slope for grasslands could be partly attributed to the large radius (>10 km) used for the extraction of OCO-2 SIF for both C_3 and C_4 species. The slope of the SIF–GPP relationship for grasslands could be altered should more SIF observations be available. We found that applying a biome-specific GPP–SIF relationship showed no advantage over using a universal GPP–SIF relationship in estimating GPP at four EC flux sites. Such a universal relationship can be more useful than biome-specific ones. A universal relationship can be used to translate SIF to GPP without vegetation type information, which can reduce the uncertainty in GPP prediction by avoiding the uncertainty from land cover classification.

Although the slope of the SIF–GPP relationship was nearly consistent among different biomes, we also found that the C_4 grasslands and croplands had a significantly higher slope than C_3 grasslands and croplands. This is consistent with the findings of two recent studies (Liu et al., 2017; Wood et al., 2017). Liu et al. (2017) conducted ground-based measurements to examine the SIF–GPP relationship, and found that slope for C_3 wheat was less than half of that for C_4 maize. Based on OCO-2 SIF and tower GPP, Wood et al. (2017) showed that the slope was significantly higher for C4 corn than for

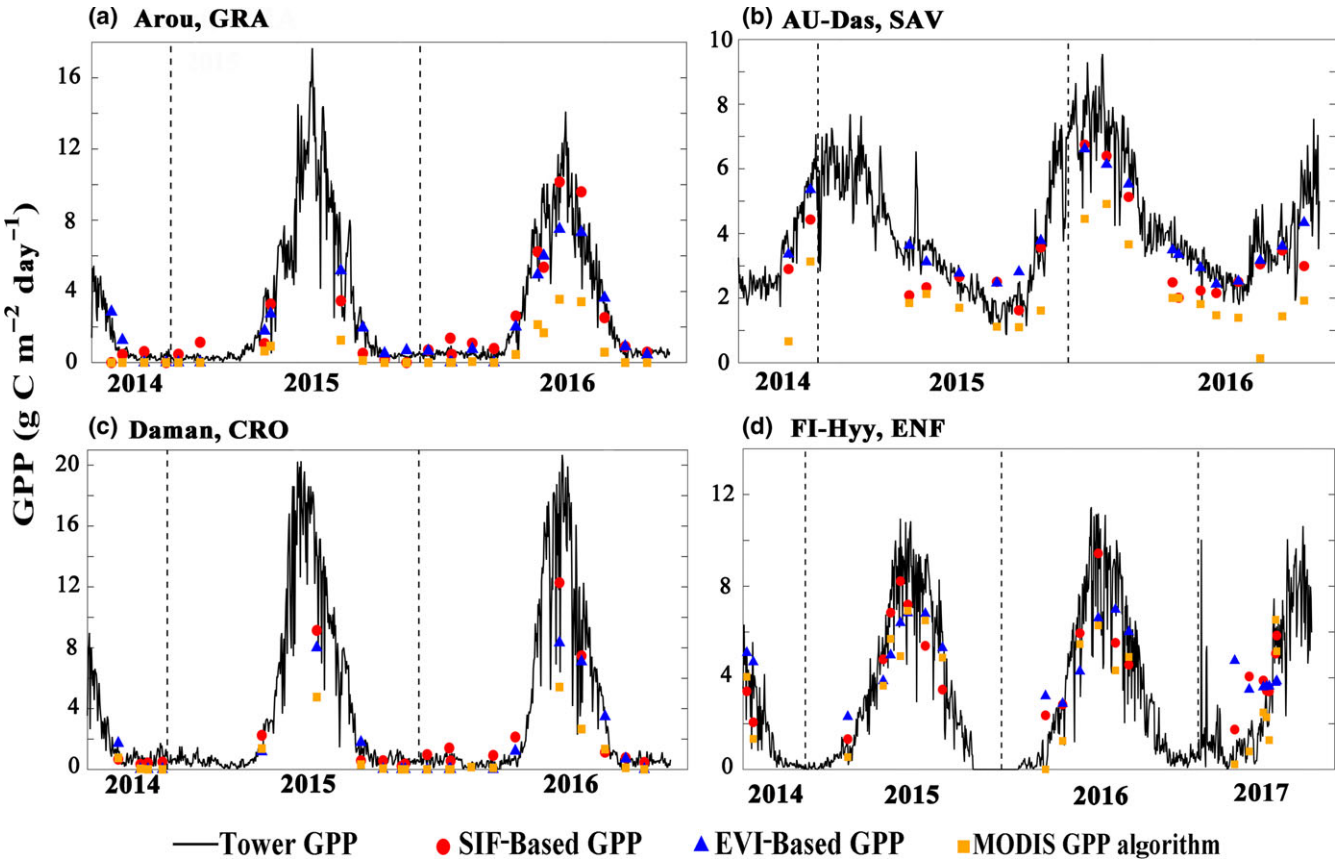

FIGURE 12 Validation of GPP estimates based on the SIF–GPP linear relationships derived from OCO-2 and flux tower data (red circles), MODIS-derived EVI_{BRDF} (blue triangles), and a light use efficiency model – the MODIS GPP algorithm (orange squares) at four selected flux sites from September 6, 2014 to December 31, 2016 (or July 31, 2017): (a) Arou, (b) AU-Das, (c) Daman, and (d) FI-Hyy [Colour figure can be viewed at wileyonlinelibrary.com]

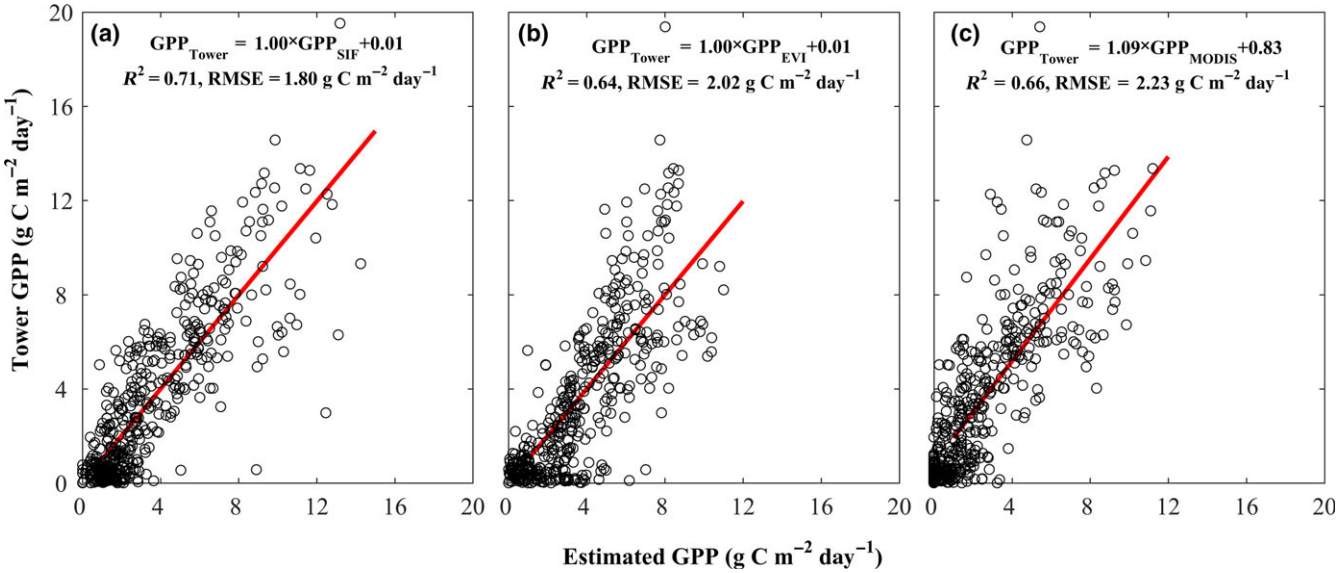

FIGURE 13 Validation of the SIF-GPP model based on the universal linear relationship between tower GPP and OCO-2 SIF (a), GPP-EVI_{BRDF} model (b), and MODIS GPP algorithm (c) for GPP estimation ($p < 0.0001$ for all three models) [Colour figure can be viewed at wileyonlinelibrary.com]

the mixed landscape dominated by both C_4 corn and C_3 soybean and grassland. Both studies indicated that C_3 and C_4 species had similar fluorescence yield (or SIF_{yield}) but had large difference in LUE_p. Plants with C_4 photosynthesis pathways are considered to have greater adaptability to high light intensity, high temperature, and dryness and therefore may exhibit higher LUEp than C_3 species

(Gitelson, Peng, Arkebauer, & Suyker, 2015; Li et al., 2006). Our current findings may support the notion that the SIF–GPP relationship is specific to the photosynthetic pathway (Liu et al., 2017). However, the much higher slope in C_4 species in this study was mainly contributed by a C_4 corn site, Daman, which alone had a very high slope (30.53 g C m^{-2} day^{-1}/W m^{-2} μm^{-1} sr^{-1}). The other C_4 site, AU-Stp, also had a relatively high slope (24.91 g C m^{-2} day^{-1}/W m^{-2} μm^{-1} sr^{-1}), although it was not significantly different from that of the C_3 sites ($p = 0.23$). The SIF–GPP relationship for C_3 versus C_4 ecosystems would be better elucidated should concurrent SIF observations and flux tower data for more grassland and cropland sites be available.

The comparison of OCO-2 SIF and MODIS VIs with tower GPP further reveals the potential of OCO-2 SIF in estimating GPP at large scales. Our results showed that OCO-2 SIF was more strongly correlated with tower GPP than were conventional NDVI and EVI, EVI_{BRDF}, and the recently proposed NIR_V. This was consistent with previous studies showing that SIF from field experiments, satellite data, or imaging spectrometer measurements could better characterize the actual photosynthesis than conventional VIs (Daumard et al., 2010; Lee et al., 2013; Rascher et al., 2015; Walther et al., 2016; Yoshida et al., 2015). Conventional VIs are largely proxies of *f*PAR and are not sensitive to rapid changes in plant physiological changes induced by environmental stresses (e.g., light, temperature, VPD) (Dobrowski, Pushnik, Zarco-Tejada, & Ustin, 2005; Zarco-Tejada et al., 2013), while SIF is emitted by the photosynthetic machinery itself and can offer a direct physiology-based measure of photosynthetic activity (Meroni et al., 2009). Unlike SIF, VIs such as NDVI and EVI do not contain information on instantaneous illumination. A fairer comparison between VIs and SIF could be achieved by either normalizing the SIF by down-welling PAR or multiplying the VIs by PAR (Frankenberg et al., 2011; Walther et al., 2016; Yoshida et al., 2015). Our results showed that the VIs × PAR had similar correlation with tower GPP as VIs alone and the correlation became weaker at the site level. This can happen when VIs, GPP, and two environmental scalars were all small, while the PAR was relatively high. The VIs × PAR could not well characterize the variation in APAR (GPP) unless the low temperature and water stresses were included. In addition, VIs, particularly NDVI, tend to be nonlinearly related to vegetation properties—saturating at high LAI (Gilabert, Sánchez-Ruiz, & Moreno, 2017; Kross, McNairn, Lapen, Sunohara, & Champagne, 2015; Nguy-Robertson et al., 2012). This saturation phenomenon was not observed in the SIF–GPP relationships found in previous studies based on satellite SIF retrievals and gridded GPP data (Frankenberg et al., 2011; Parazoo et al., 2014), recent studies based on OCO-2 SIF and flux tower data for individual sites (Li et al., 2018a; Sun et al., 2017; Wood et al., 2017), and our global analysis based on OCO-2 SIF and tower GPP from 64 sites and eight biomes.

Understanding how SIF responds to APAR and environmental factors can help reveal the underlying mechanisms of the observed strong relationship between SIF and GPP. Previous studies suggested that APAR dominated the SIF–GPP relationship, while SIF also contained information on environmental stresses that were closely associated with LUE_p (Li, Xiao, & He, 2018a; Walther et al., 2016; Yang et al., 2015, 2016). A recent study used GOME-2 SIF observations as a proxy for GPP to identify the dominant bioclimatic control factors (e.g., VPD, Tmin, soil moisture) that influence primary productivity (Madani et al., 2017). For our selected two EC flux sites with different environmental controls on photosynthesis, we found that SIF responded to APAR and environmental factors (*f*Tmin for FI-Hyy site and *f*VPD for AU-Das site) in a similar manner as GPP, further demonstrating the close relationship between GPP and SIF. Our results showed that SIF was mainly driven by APAR and was also influenced by environmental stresses (temperature limitation and water stress) that control LUE_p across a number of sites and a variety of biomes over the globe, highlighting that SIF could respond well to these bioclimatic and environmental factors at the ecosystem scale. This encourages wide application of OCO-2 SIF in both estimating GPP and examining the effects of environmental stresses on terrestrial photosynthesis.

Despite the substantial value and potential of OCO-2 SIF in assessing terrestrial photosynthesis and its responses to environmental stresses for a variety of biomes, more extensive applications of OCO-2 SIF in carbon cycling studies still face challenges. Due to the sparse global coverage of OCO-2, temporally dense SIF retrievals (e.g., more than 10 daily observations per site over the 2014–2016 period) are not available for the majority of the EC flux sites over the globe. Therefore, it is not yet feasible to examine the seasonal or interannual variations in photosynthesis or to detect vegetation phenology at the ecosystem scale using OCO-2 SIF observations. It is also challenging to use OCO-2 SIF data to examine photosynthesis or its response to environmental stresses at regional or global scales due to the spatially and temporally sparse nature of OCO-2 data. One possible solution is to generate spatially and temporally continuous SIF estimates with moderate resolution by merging OCO-2 SIF soundings with other moderate-resolution satellite datasets that are spatially and temporally continuous (e.g., MODIS) (Li et al., 2018a). Another possible solution is to make use of the advantages of both OCO-2 (finer resolution, higher quality) and GOME-2 (spatially and temporally continuous coverage) data. For example, OCO-2 data is likely to be useful for calibrating GOME-2 data, leading to a calibrated, higher quality SIF dataset that is spatially and temporally continuous. OCO-2 SIF data can also be synergistically used with SIF from other ongoing or upcoming missions such as the TROPOspheric Monitoring Instrument (TROPOMI), OCO-3, GOSAT-2, or the FLuorescence EXplorer (FLEX). In particular, the TROPOMI instrument on board Sentinel-5P that launched in October 2017 will enable the retrievals of continuous global SIF at a spatial grid size of 0.1° (Guanter et al., 2015), and the FLEX that will be launched in 2022 is specifically designed for mapping SIF at a spatial resolution of 300 m (Drusch et al., 2017). These SIF data along with OCO-2 SIF will likely open up a new era in terrestrial carbon cycle studies. The universal, robust relationship between OCO-2 SIF and tower GPP across a large number of sites and a wide variety of biomes demonstrated in this study will be useful for translating the finer-resolution SIF maps from TROPOMI and FLEX to gridded, finer-resolution GPP estimates (300 m—0.1°) at regional to global scales. The resulting gridded GPP estimates will be valuable for assessing ecosystem carbon

uptake and plant productivity at various spatial and temporal scales, comparing against gridded GPP upscaled from FLUXNET observations (e.g., Xiao et al., 2010, 2014), and benchmarking terrestrial biosphere models (e.g., Ito et al., 2017; Thorn, Xiao, & Ollinger, 2015).

5 | SUMMARY

Our study presents the first global analysis of the relationship between SIF and GPP at the ecosystem scale based on OCO-2 SIF and tower GPP data for a total of 64 EC flux sites encompassing eight major biomes across the globe. The OCO-2 SIF showed strong correlations with tower GPP (R^2 = 0.48–0.72, $p < 0.0001$) in both SIF retrieval bands (757 and 771 nm) and at two timescales (midday and daily), with the strongest relationship observed in the 757 nm band (SIF_{757}) at the daily timescale (R^2 = 0.72, $p < 0.0001$). The SIF-GPP relationship did not significantly vary with the measurement mode at both midday and daily timescales. OCO-2 SIF_{757} exhibited much stronger correlation with tower GPP than MODIS-derived NDVI, EVI, and NIR_V and slightly stronger relationship with tower GPP than BRDF-corrected EVI (EVI_{BRDF}: R^2 = 0.64, $p < 0.0001$) and NIR (NIR_{V_BRDF}: R^2 = 0.65, $p < 0.0001$). The OCO-2 SIF_{757} had better predictive ability in GPP estimation than EVI_{BRDF} and a light use efficiency model (the MODIS GPP algorithm). We further found that the SIF was mainly driven by APAR and was also influenced by environmental stresses (temperature and water stresses) related to LUE_p. SIF responded to APAR and environmental scaling factors (fT_{min} and fVPD) in the same manner as GPP at two representative flux sites with different environmental controls on photosynthesis. The strong SIF–GPP relationship was found for all eight biomes (R^2 = 0.57–0.79, $p < 0.0001$) except evergreen broadleaf forests (R^2 = 0.16, $p < 0.05$). The slope of the SIF–GPP relationship was generally consistent among biomes, which indicates that a nearly universal relationship between SIF and GPP exists across a wide variety of biomes. The nearly universal SIF–GPP relationship can be used to translate SIF to GPP as effectively as biome-specific relationships at the site level and can potentially lead to more accurate GPP estimates regionally or globally by avoiding the uncertainty from land cover classification.

Our study demonstrated the substantial value and potential of OCO-2 SIF in carbon cycling studies. Future work based on more SIF observations and/or process-based modeling will be helpful for evaluating the universal SIF–GPP relationship across a variety of biomes as suggested by our findings. Synergistic uses of OCO-2 SIF with other spatially and temporally continuous remote sensing products (e.g., MODIS) and SIF observations from other missions (e.g., GOME-2, GOSAT, TROPOMI, FLEX) will open up a new era for ecosystem functioning and carbon cycling studies and benchmarking of terrestrial biosphere models.

ACKNOWLEDGEMENTS

This study was supported by the National Aeronautics and Space Administration (NASA) (Carbon Cycle Science Program: Grant No. NNX14AJ18G; Climate Indicators and Data Products for Future National Climate Assessments: Grant No. NNX16AG61G), National Science Foundation (MacroSystems Biology Program: Grant Nos. 1065777, 1638688), Iola Hubbard Climate Change Endowment, National Natural Science Foundation of China (Grant Nos. 41471293 and 41671361), and China Scholarship Council. We thank the OCO-2 and MODIS science teams for making OCO-2 SIF and MODIS data available. We also acknowledge the investigators who provided flux tower data and are not coauthoring this manuscript: Arou, Daman, Dashalong & HZZ: Ziwei Xu, Shaomin Liu, & Xufeng Wang; BE-Lon: Anne DeLigne; CH-Cha: Kathrin Fuchs; CH-Cha & CH-Fru: Nina Buchmann; CH-Fru: Lutz Merbold; CH-Lae: Eugenie Limoges; DK-Sor: Andreas Lbrom and Kim Pilegaard; FI-VAR: Pasi Kolari; NL-Loo: Eddy Moors; PT-Cor: Filipe Costa e Silva; PT-Tcz: Marek Urbaniak; US-CZ1, US-CZ4 & US-Scs: Michael Goulden; US-KLS: Nathaniel A. Brunsell; US-NR1: Sean Burns and Peter Blanken; US-Slt: Kenneth L. Clark; US-SRC: Shirley Papuga; US-SRG & US-SRM: Russell Scott; USTWT, US-TW3 & US-VAR: Dennis D. Baldocchi, Elke Eichelmann, Siyan Ma; US-WWT, US-ME2 & US-ME6: Beverly E. Law. We thank the two anonymous reviewers for their constructive and insightful comments on the manuscript.

AUTHOR CONTRIBUTION

J. Xiao and X. Li designed the research. X. Li processed the data. X. Li and J. Xiao analyzed the data and wrote the paper. B. He provided comments and suggestions on the manuscript. M.A. Arain, J. Beringer, A.R. Desai, C. Emmel, D.Y. Hollinger, A. Krasnova, I. Mammarella, S.M. Noe, P.S. Ortiz, A.C. Rey-Sanchez, A.V. Rocha, and A. Varlagin provided flux data and comments and are listed alphabetically.

ORCID

Jingfeng Xiao http://orcid.org/0000-0002-0622-6903
Steffen M. Noe http://orcid.org/0000-0003-1514-1140

REFERENCES

Badgley, G., Field, C. B., & Berry, J. A. (2017). Canopy near-infrared reflectance and terrestrial photosynthesis. *Science Advances*, *3*, e1602244. https://doi.org/10.1126/sciadv.1602244

Baker, N. R. (2008). Chlorophyll fluorescence: a probe of photosynthesis *in vivo*. *Annual Review of Plant Biology*, *59*, 89–113. https://doi.org/10.1146/annurev.arplant.59.032607.092759

Dai, Z., Edwards, G. E., & Ku, M. S. (1992). Control of photosynthesis and stomatal conductance in Ricinus communis L. (castor bean) by leaf to air vapor pressure deficit. *Plant Physiology*, *99*, 1426–1434. https://doi.org/10.1104/pp.99.4.1426

Damm, A., Guanter, L., Verhoef, W., Schläpfer, D., Garbari, S., & Schaepman, M. (2015). Impact of varying irradiance on vegetation indices and chlorophyll fluorescence derived from spectroscopy data. *Remote Sensing of Environment*, *156*, 202–215. https://doi.org/10.1016/j.rse.2014.09.031

Daumard, F., Champagne, S., Fournier, A., Goulas, Y., Ounis, A., Hanocq, J.-F., & Moya, I. (2010). A field platform for continuous measurement

of canopy fluorescence. *IEEE Transactions on Geoscience and Remote Sensing*, *48*, 3358–3368. https://doi.org/10.1109/TGRS.2010.2046420

Desai, A. R., Richardson, A. D., Moffat, A. M., Kattge, J., Hollinger, D. Y., Barr, A., … Reichstein, M. (2008). Cross-site evaluation of eddy covariance GPP and RE decomposition techniques. *Agricultural and Forest Meteorology*, *148*, 821–838. https://doi.org/10.1016/j.agrformet.2007.11.012

Dobrowski, S., Pushnik, J., Zarco-Tejada, P., & Ustin, S. (2005). Simple reflectance indices track heat and water stress-induced changes in steady-state chlorophyll fluorescence at the canopy scale. *Remote Sensing of Environment*, *97*, 403–414. https://doi.org/10.1016/j.rse.2005.05.006

Dong, J., Xiao, X., Wagle, P., Zhang, G., Zhou, Y., Jin, C., … Wang, J. (2015). Comparison of four EVI-based models for estimating gross primary production of maize and soybean croplands and tallgrass prairie under severe drought. *Remote Sensing of Environment*, *162*, 154–168. https://doi.org/10.1016/j.rse.2015.02.022

Drusch, M., Moreno, J., Del Bello, U., Franco, R., Goulas, Y., Huth, A., … Mohammed, G. (2017). The FLuorescence EXplorer Mission Concept—ESA's Earth Explorer 8. *IEEE Transactions on Geoscience and Remote Sensing*, *55*, 1273–1284. https://doi.org/10.1109/TGRS.2016.2621820

Frankenberg, C., Fisher, J. B., Worden, J., Badgley, G., Saatchi, S. S., Lee, J. E., … Kuze, A. (2011). New global observations of the terrestrial carbon cycle from GOSAT: Patterns of plant fluorescence with gross primary productivity. *Geophysical Research Letters*, *38*, L17706. https://doi.org/10.1029/2011GL048738

Frankenberg, C., O'Dell, C., Berry, J., Guanter, L., Joiner, J., Köhler, P., … Taylor, T. E. (2014). Prospects for chlorophyll fluorescence remote sensing from the Orbiting Carbon Observatory-2. *Remote Sensing of Environment*, *147*, 1–12. https://doi.org/10.1016/j.rse.2014.02.007

Gilabert, M. A., Sánchez-Ruiz, S., & Moreno, Á. (2017). Annual Gross Primary Production from Vegetation Indices: A Theoretically Sound Approach. *Remote Sensing*, *9*, 193. https://doi.org/10.3390/rs9030193

Gitelson, A. A., Peng, Y., Arkebauer, T. J., & Suyker, A. E. (2015). Productivity, absorbed photosynthetically active radiation, and light use efficiency in crops: Implications for remote sensing of crop primary production. *Journal of Plant Physiology*, *177*, 100–109. https://doi.org/10.1016/j.jplph.2014.12.015

Grace, J., Nichol, C., Disney, M., Lewis, P., Quaife, T., & Bowyer, P. (2007). Can we measure terrestrial photosynthesis from space directly, using spectral reflectance and fluorescence? *Global Change Biology*, *13*, 1484–1497. https://doi.org/10.1111/j.1365-2486.2007.01352.x

Guanter, L., Aben, I., Tol, P., Krijger, J., Hollstein, A., Köhler, P., … Landgraf, J. (2015). Potential of the TROPOspheric Monitoring Instrument (TROPOMI) onboard the Sentinel-5 Precursor for the monitoring of terrestrial chlorophyll fluorescence. *Atmospheric Measurement Techniques*, *8*, 1337–1352. https://doi.org/10.5194/amt-8-1337-2015

Guanter, L., Frankenberg, C., Dudhia, A., Lewis, P. E., Gómez-Dans, J., Kuze, A., … Grainger, R. G. (2012). Retrieval and global assessment of terrestrial chlorophyll fluorescence from GOSAT space measurements. *Remote Sensing of Environment*, *121*, 236–251. https://doi.org/10.1016/j.rse.2012.02.006

Guanter, L., Zhang, Y., Jung, M., Joiner, J., Voigt, M., Berry, J. A., … Lee, J.-E. (2014). Global and time-resolved monitoring of crop photosynthesis with chlorophyll fluorescence. *Proceedings of the National Academy of Sciences*, *111*, E1327–E1333. https://doi.org/10.1073/pnas.1320008111

Hayek, M. N., Wehr, R., Longo, M., Hutyra, L. R., Wiedemann, K., Munger, J. W., … Wofsy, S. C. (2018). A novel correction for biases in forest eddy covariance carbon balance. *Agricultural and Forest Meteorology*, *250*, 90–101. https://doi.org/10.1016/j.agrformet.2017.12.186

Ito, A., Nishina, K., Reyer, C. P. O., François, L., Henrot, A. J., Munhoven, G., … Zhao, F. (2017). Photosynthetic productivity and its efficiencies in ISIMIP2a biome models: Benchmarking for impact assessment studies. *Environmental Research Letters*, *12*, 085001. https://doi.org/10.1088/1748-9326/aa7a19

Jeong, S.-J., Schimel, D., Frankenberg, C., Drewry, D. T., Fisher, J. B., Verma, M., … Joiner, J. (2017). Application of satellite solar-induced chlorophyll fluorescence to understanding large-scale variations in vegetation phenology and function over northern high latitude forests. *Remote Sensing of Environment*, *190*, 178–187. https://doi.org/10.1016/j.rse.2016.11.021

Joiner, J., Guanter, L., Lindstrot, R., Voigt, M., Vasilkov, A., Middleton, E., … Frankenberg, C. (2013). Global monitoring of terrestrial chlorophyll fluorescence from moderate spectral resolution near-infrared satellite measurements: Methodology, simulations, and application to GOME-2. *Atmospheric Measurement Techniques*, *6*, 2803–2823. https://doi.org/10.5194/amt-6-2803-2013

Joiner, J., Yoshida, Y., Vasilkov, A., & Middleton, E. (2011). First observations of global and seasonal terrestrial chlorophyll fluorescence from space. *Biogeosciences*, *8*, 637–651. https://doi.org/10.5194/bg-8-637-2011

Joiner, J., Yoshida, Y., Vasilkov, A., Schaefer, K., Jung, M., Guanter, L., … Huemmrich, K. (2014). The seasonal cycle of satellite chlorophyll fluorescence observations and its relationship to vegetation phenology and ecosystem atmosphere carbon exchange. *Remote Sensing of Environment*, *152*, 375–391. https://doi.org/10.1016/j.rse.2014.06.022

Koffi, E., Rayner, P., Norton, A., Frankenberg, C., & Scholze, M. (2015). Investigating the usefulness of satellite-derived fluorescence data in inferring gross primary productivity within the carbon cycle data assimilation system. *Biogeosciences*, *12*, 4067–4084. https://doi.org/10.5194/bg-12-4067-2015

Kross, A., McNairn, H., Lapen, D., Sunohara, M., & Champagne, C. (2015). Assessment of RapidEye vegetation indices for estimation of leaf area index and biomass in corn and soybean crops. *International Journal of Applied Earth Observation and Geoinformation*, *34*, 235–248.

Lee, J.-E., Frankenberg, C., van der Tol, C., Berry, J. A., Guanter, L., Boyce, C. K., … Asefi, S. (2013). Forest productivity and water stress in Amazonia: Observations from GOSAT chlorophyll fluorescence. *Proceedings of the Royal Society of London B: Biological Sciences*, *280*, 20130171. https://doi.org/10.1098/rspb.2013.0171

Li, X., Xiao, J., & He, B. (2018a). Chlorophyll fluorescence observed by OCO-2 is strongly related to gross primary productivity estimated from flux towers in temperate forests. *Remote Sensing of Environment*, *204*, 659–671. https://doi.org/10.1016/j.rse.2017.09.034

Li, X., Xiao, J., & He, B. (2018b). Higher absorbed solar radiation partly offset the negative effects of water stress on the photosynthesis of Amazon forests during the 2015 drought. *Environmental Research Letters*, *13*, 044005. https://doi.org/10.1088/1748-9326/aab0b1

Li, J., Yu, Q., Sun, X., Tong, X., Ren, C., Wang, J., … Yu, G. (2006). Carbon dioxide exchange and the mechanism of environmental control in a farmland ecosystem in North China Plain. *Science in China Series D: Earth Sciences*, *49*, 226–240. https://doi.org/10.1007/s11430-006-8226-1

Liu, L., Guan, L., & Liu, X. (2017). Directly estimating diurnal changes in GPP for C3 and C4 crops using far-red sun-induced chlorophyll fluorescence. *Agricultural and Forest Meteorology*, *232*, 1–9. https://doi.org/10.1016/j.agrformet.2016.06.014

Madani, N., Kimball, J. S., Jones, L. A., Parazoo, N. C., & Guan, K. (2017). Global analysis of bioclimatic controls on ecosystem productivity using satellite observations of solar-induced chlorophyll fluorescence. *Remote Sensing*, *9*, 530. https://doi.org/10.3390/rs9060530

Mäkelä, A., Kolari, P., Karimäki, J., Nikinmaa, E., Perämäki, M., & Hari, P. (2006). Modelling five years of weather-driven variation of GPP in a

boreal forest. *Agricultural and Forest Meteorology*, *139*, 382–398. https://doi.org/10.1016/j.agrformet.2006.08.017

Meroni, M., Rossini, M., Guanter, L., Alonso, L., Rascher, U., Colombo, R., & Moreno, J. (2009). Remote sensing of solar-induced chlorophyll fluorescence: Review of methods and applications. *Remote Sensing of Environment*, *113*, 2037–2051. https://doi.org/10.1016/j.rse.2009.05.003

Monteith, J. (1972). Solar radiation and productivity in tropical ecosystems. *Journal of Applied Ecology*, *9*, 747–766. https://doi.org/10.2307/2401901

Monteith, J. L., & Moss, C. (1977). Climate and the efficiency of crop production in Britain [and discussion]. *Philosophical Transactions of the Royal Society of London B: Biological Sciences*, *281*, 277–294. https://doi.org/10.1098/rstb.1977.0140

Nguy-Robertson, A., Gitelson, A., Peng, Y., Viña, A., Arkebauer, T., & Rundquist, D. (2012). Green leaf area index estimation in maize and soybean: Combining vegetation indices to achieve maximal sensitivity. *Agronomy Journal*, *104*, 1336–1347.

Öquist, G. (1983). Effects of low temperature on photosynthesis. *Plant, Cell & Environment*, *6*, 281–300.

Papale, D., Reichstein, M., Aubinet, M., Canfora, E., Bernhofer, C., Kutsch, W., … Vesala, T. (2006). Towards a standardized processing of Net Ecosystem Exchange measured with eddy covariance technique: Algorithms and uncertainty estimation. *Biogeosciences*, *3*, 571–583. https://doi.org/10.5194/bg-3-571-2006

Parazoo, N. C., Bowman, K., Fisher, J. B., Frankenberg, C., Jones, D., Cescatti, A., … Montagnani, L. (2014). Terrestrial gross primary production inferred from satellite fluorescence and vegetation models. *Global Change Biology*, *20*, 3103–3121. https://doi.org/10.1111/gcb.12652

Porcar-Castell, A., Tyystjärvi, E., Atherton, J., van der Tol, C., Flexas, J., Pfündel, E. E., … Berry, J. A. (2014). Linking chlorophyll a fluorescence to photosynthesis for remote sensing applications: Mechanisms and challenges. *Journal of Experimental Botany*, *65*, 4065–4095. https://doi.org/10.1093/jxb/eru191

Rascher, U., Alonso, L., Burkart, A., Cilia, C., Cogliati, S., Colombo, R., … Hanus, J. (2015). Sun-induced fluorescence–a new probe of photosynthesis: First maps from the imaging spectrometer HyPlant. *Global Change Biology*, *21*, 4673–4684. https://doi.org/10.1111/gcb.13017

Reichstein, M., Falge, E., Baldocchi, D., Papale, D., Aubinet, M., Berbigier, P., … Granier, A. (2005). On the separation of net ecosystem exchange into assimilation and ecosystem respiration: Review and improved algorithm. *Global Change Biology*, *11*, 1424–1439. https://doi.org/10.1111/j.1365-2486.2005.001002.x

Rogers, C. D. W., & Beringer, J. (2017). Describing rainfall in northern Australia using multiple climate indices. *Biogeosciences*, *14*, 597. https://doi.org/10.5194/bg-14-597-2017

Running, S. W., Nemani, R. R., Heinsch, F. A., Zhao, M., Reeves, M., & Hashimoto, H. (2004). A continuous satellite-derived measure of global terrestrial primary production. *BioScience*, *54*, 547–560. https://doi.org/10.1641/0006-3568(2004)054[0547:ACSMOG]2.0.CO;2

Schmid, H. P. (2002). Footprint modeling for vegetation atmosphere exchange studies: A review and perspective. *Agricultural and Forest Meteorology*, *113*, 159–183. https://doi.org/10.1016/S0168-1923(02)00107-7

Sims, D. A., Rahman, A. F., Cordova, V. D., El-Masri, B. Z., Baldocchi, D. D., Flanagan, L. B., … Monson, R. K. (2006). On the use of MODIS EVI to assess gross primary productivity of North American ecosystems. *Journal of Geophysical Research: Biogeosciences*, *111*. https://doi.org/10.1029/2006JG000162

Sjöström, M., Ardö, J., Arneth, A., Boulain, N., Cappelaere, B., Eklundh, L., … Nouvellon, Y. (2011). Exploring the potential of MODIS EVI for modeling gross primary production across African ecosystems. *Remote Sensing of Environment*, *115*, 1081–1089. https://doi.org/10.1016/j.rse.2010.12.013

Sun, Y., Frankenberg, C., Jung, M., Joiner, J., Guanter, L., Köhler, P., & Magney, T. (2018). Overview of Solar-Induced chlorophyll Fluorescence (SIF) from the Orbiting Carbon Observatory-2: Retrieval, cross-mission comparison, and global monitoring for GPP. *Remote Sensing of Environment*, https://doi.org/10.1016/j.rse.2018.02.016

Sun, Y., Frankenberg, C., Wood, J. D., Schimel, D., Jung, M., Guanter, L., … Griffis, T. J. (2017). OCO-2 advances photosynthesis observation from space via solar-induced chlorophyll fluorescence. *Science*, *358*, eaam5747. https://doi.org/10.1126/science.aam5747

Sun, Y., Fu, R., Dickinson, R., Joiner, J., Frankenberg, C., Gu, L., … Fernando, N. (2015). Drought onset mechanisms revealed by satellite solar-induced chlorophyll fluorescence: Insights from two contrasting extreme events. *Journal of Geophysical Research: Biogeosciences*, *120*, 2427–2440.

Tang, H., & Dubayah, R. (2017). Light-driven growth in Amazon evergreen forests explained by seasonal variations of vertical canopy structure. *Proceedings of the National Academy of Sciences*, *114*, 2640–2644.

Tardieu, F. (2013). Plant response to environmental conditions: Assessing potential production, water demand, and negative effects of water deficit. *Frontiers in Physiology*, *4*, 17.

Thorn, A. M., Xiao, J., & Ollinger, S. V. (2015). Generalization and evaluation of the process-based forest ecosystem model PnET-CN for other biomes. *Ecosphere*, *6*(3), 43. https://doi.org/10.1890/ES14-00542.1

Verma, M., Schimel, D., Evans, B., Frankenberg, C., Beringer, J., Drewry, D. T., … Moore, C. (2017). Effect of environmental conditions on the relationship between solar induced fluorescence and gross primary productivity at an OzFlux grassland site. *Journal of Geophysical Research: Biogeosciences*, *122*, 716–733.

Walther, S., Voigt, M., Thum, T., Gonsamo, A., Zhang, Y., Köhler, P., … Guanter, L. (2016). Satellite chlorophyll fluorescence measurements reveal large-scale decoupling of photosynthesis and greenness dynamics in boreal evergreen forests. *Global Change Biology*, *22*, 2979–2996. https://doi.org/10.1111/gcb.13200

Wood, J. D., Griffis, T. J., Baker, J. M., Frankenberg, C., Verma, M., & Yuen, K. (2017). Multiscale analyses of solar-induced florescence and gross primary production. *Geophysical Research Letters*, *44*, 533–541. https://doi.org/10.1002/2016GL070775

Xiao, J., & Moody, A. (2005). Geographical distribution of global greening trends and their climatic correlates: 1982-1998. *International Journal of Remote Sensing*, *26*, 2371–2390. https://doi.org/10.1080/01431160500033682

Xiao, J., Ollinger, S. V., Frolking, S., Hurtt, G. C., Hollinger, D. Y., Davis, K. J., … Suyker, A. E. (2014). Data-driven diagnostics of terrestrial carbon dynamics over North America. *Agricultural and Forest Meteorology*, *197*, 142–157. https://doi.org/10.1016/j.agrformet.2014.06.013

Xiao, J., Zhuang, Q., Law, B. E., Chen, J., Baldocchi, D. D., Cook, D. R., … Ma, S. (2010). A continuous measure of gross primary production for the conterminous United States derived from MODIS and AmeriFlux data. *Remote Sensing of Environment*, *114*, 576–591. https://doi.org/10.1016/j.rse.2009.10.013

Yang, X., Tang, J., Mustard, J. F., Lee, J. E., Rossini, M., Joiner, J., … Richardson, A. D. (2015). Solar-induced chlorophyll fluorescence that correlates with canopy photosynthesis on diurnal and seasonal scales in a temperate deciduous forest. *Geophysical Research Letters*, *42*, 2977–2987. https://doi.org/10.1002/2015GL063201

Yang, H., Yang, X., Zhang, Y., Heskel, M. A., Lu, X., Munger, J. W., … Tang, J. (2016). Chlorophyll fluorescence tracks seasonal variations of photosynthesis from leaf to canopy in a temperate forest. *Global Change Biology*, *23*, 2874–2886.

Yoshida, Y., Joiner, J., Tucker, C., Berry, J., Lee, J.-E., Walker, G., … Wang, Y. (2015). The 2010 Russian drought impact on satellite measurements of solar-induced chlorophyll fluorescence: Insights from modeling and comparisons with parameters derived from satellite

reflectances. *Remote Sensing of Environment*, *166*, 163–177. https://doi.org/10.1016/j.rse.2015.06.008

Zarco-Tejada, P. J., Morales, A., Testi, L., & Villalobos, F. J. (2013). Spatio-temporal patterns of chlorophyll fluorescence and physiological and structural indices acquired from hyperspectral imagery as compared with carbon fluxes measured with eddy covariance. *Remote Sensing of Environment*, *133*, 102–115. https://doi.org/10.1016/j.rse.2013.02.003

Zhang, Y., Guanter, L., Berry, J. A., Joiner, J., van der Tol, C., Huete, A., … Köhler, P. (2014). Estimation of vegetation photosynthetic capacity from space-based measurements of chlorophyll fluorescence for terrestrial biosphere models. *Global Change Biology*, *20*, 3727–3742. https://doi.org/10.1111/gcb.12664

Zhang, Y., Xiao, X., Jin, C., Dong, J., Zhou, S., Wagle, P., … Zhang, G. (2016). Consistency between sun-induced chlorophyll fluorescence and gross primary production of vegetation in North America. *Remote Sensing of Environment*, *183*, 154–169. https://doi.org/10.1016/j.rse.2016.05.015

SUPPORTING INFORMATION

Additional supporting information may be found online in the Supporting Information section at the end of the article.

How to cite this article: Li X, Xiao J, He B, et al. Solar-induced chlorophyll fluorescence is strongly correlated with terrestrial photosynthesis for a wide variety of biomes: First global analysis based on OCO-2 and flux tower observations. *Glob Change Biol*. 2018;24:3990–4008. https://doi.org/10.1111/gcb.14297